arXiv:1609.09010v1 [math.OC] 28 Sep 2016

# Estimation of Graphical Models through Structured Norm Minimization

Davoud Ataee Tarzanagh* George Michailidis†

**Abstract**

We study the problem of estimating a multi-structured graphical model from high dimensional data, where the ground-truth structure can *simultaneously* contains hubs, dense subgraphs, as well as sparse components. This problem is motivated by applications in several fields, including molecular biology, finance and political science, where the underlying networks exhibit structure that is more involved than simple sparsity. We introduce a general framework that allows such decompositions for estimating Markov Random Fields and covariances from high-dimensional data. The resulting optimization problem is convex and we introduce a multi-block Alternating Direction Method of Multipliers (ADMM) to solve it efficiently. Further, we show that the iterative sequence generated by the ADMM converges to a stationary point of the associated augmented Lagrangian function. We illustrate the superior performance of the proposed framework on a number of synthetic data sets generated from both random and structured networks. Further, we apply the method to a number of real data sets and discuss the results.

Markov random field, Gaussian covariance graph model, penalty, Alternating direction method of multipliers (ADMM), convergence.

## 1 Introduction

There is a substantial body of literature on methods for estimating network structures from high-dimensional data, motivated by important biomedical and social science applications [2, 33, 45, 21, 9, 49, 19]. Two powerful formalisms have been employed for this task, the Markov Random Field (MRF) model and the Gaussian covariance graph model (GCGM). The former captures statistical conditional dependence relationships amongst random variables that correspond to the network nodes, while the latter to marginal associations. Since in most applications the number of model parameters to be estimated far exceeds the available sample size, the assumption of sparsity is made and imposed through regularization. An $\ell_1$ penalty on the parameters encoding the network edges is the most common choice [17, 53, 29, 6, 52], which can also be interpreted from the Bayesian perspective as using an independent double-exponential prior distribution on each edge parameter. Consequently, this approach encourages sparse uniform network structures that may not be the most suitable choice for many real world applications which in turn have hub nodes or dense subgraphs. As argued in [2, 33, 39, 32, 16, 40] many networks exhibit different structures at different scales. An example includes a densely connected subgraph, also known as a community in the social networks literature. Such structures in social interaction networks may correspond to groups of people sharing common interests or being co-located [50, 41], while in biological systems to groups of proteins responsible for regulating or synthesizing chemical products [18, 31](see, Figure 2 for two eaxplmes).

To detect densely connected components in networks estimated from high-dimensional data, recent work has focused on developing models exhibiting *structured sparsity* [36, 11, 24, 49]. However, the proposed methods can

*Department of Mathematics & UF Informatics Institute, University of Florida, Emails: tarzanagh@ufl.edu
†Department of Statistics & UF Informatics Institute, University of Florida, Email: gmichail@ufl.edu

not accommodate multiple structures within a network. In turn, the unified framework introduced next, can estimate from high-dimensional data such structures, including *hubs* and *dense subgraphs*, where the size and location of such structures is not known a *priori*. To achieve this goal, it leverages a new structured norm that is used as the regularization term of the corresponding objective function. Further, we consider an efficient ADMM algorithm and establish its global convergence. The algorithm takes advantage of the special structure of the problem formulation and thus is suitable for large instances of the problem.

The remainder of the paper is organized as follows: In Section 2, we present the new structured norm used as the regularization term in the objective function of the Random Markov Field and covariance graph models. In Section 3, we introduce an efficient multi-block ADMM algorithm for estimating structured graphical models, and provide a detailed convergence analysis of our new algorithm. In Section 4, we illustrate the proposed framework on a number of data sets, while some concluding remarks are drawn in Section 5.

## 2 A Framework for Learning under Structured Sparsity

We start by introducing key definitions and associated notation.

We introduce the notion of symmetric group-support and group-support recovery results [42, 49]. Using correspondence theory, we define a norm for symmetric structured sparsity, whose support are unions of symmetric overlapping groups of variables.

Define a group $G$ as a set of indices that is a subset of $[p] \times [p]$. Let

$$\mathscr{G} := \{G_1, G_2, \ldots, G_{\aleph}\}, \quad \text{s. t.} \quad \bigcup_{\iota=1}^{\aleph} G_\iota = \{(1,1), \ldots, (1,p), \ldots, (p,p)\},$$

that is, a spanning set of subsets of $\{(1,1), \ldots, (1,p), \ldots, (p,p)\}$. Note that $\mathscr{G}$ is a set of groups which is not necessarily a partition of $[p] \times [p]$, and therefore, it is possible for elements of $\mathscr{G}$ to overlap (see, Figure 1). Let

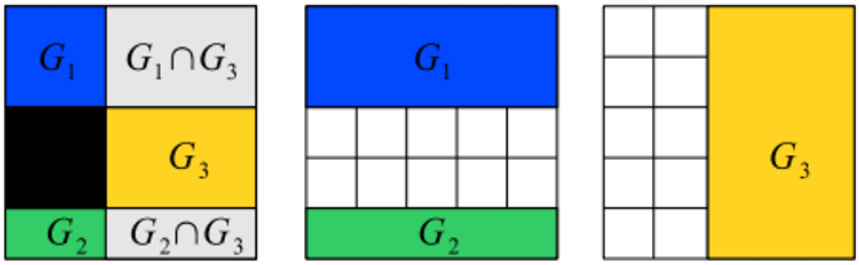


Figure 1: Groups and induced overlap pattern: three sparsity-inducing groups (middle and right panels) denoted by $G_1$, $G_2$ and $G_3$. Overlap of groups (left panel), denoted by $G_1 \bigcap G_2$ and $G_2 \bigcap G_3$ [38].

$card(G_\iota) = r^\iota$ for $\iota = 1, \ldots, \aleph$, where $card(\cdot)$ denotes the cardinality of a set. We will associate with every group $G_\iota$, a linear operator $\mathscr{A}_\iota : \mathbb{R}^{r^\iota} \to \mathbb{R}^{p \times p}$, such that for $v \in \mathbb{R}^{r^\iota}$, $\mathscr{A}_\iota(v)$ is supported on group $G_\iota$.

**Definition 1** *A symmetric matrix $\Theta$ is said to have a symmetric structure under $\mathscr{G}$, if it can be expressed as $\Theta = W + W^T$ where the support of $W$ is a subset of a union of groups in $\mathscr{G}$.*

Let $\Theta$ be a $p \times p$ symmetric matrix containing the parameters of interest. Let for all $(i, j) \in G$, we have that $i \leq j$. Thus, a matrix that is supported on a group $G$ is upper triangular. Given a set of groups $\mathscr{G}$, we would like to define a

norm that promotes matrices $\Theta$ that can be expressed as

$$\mathscr{A}_{\bar{\imath}}(W_{\bar{\imath}}) + \mathscr{A}_{\bar{\imath}}(W_{\bar{\imath}})^T + \sum_{\imath=1}^{\aleph} \mathscr{A}_\imath(W_\imath) + \mathscr{A}_\imath(W_\imath)^T,$$

where $\mathscr{A}_{\bar{\imath}}(W_{\bar{\imath}})$ is a sparse matrix under the group $G_{\bar{\imath}}$ and $\mathscr{A}_\imath(W_\imath)$ is a structured matrix under $G_\imath$ for $\imath = 1, \ldots, \aleph$.

**Definition 2** *The symmetric overlap norm for a set of groups $\mathscr{G}$ is given by,*

$$\begin{aligned} \Psi^{\mathscr{G}}(\Theta) := \underset{\mathscr{A}_\imath(W_\imath),\ \mathscr{A}_{\bar{\imath}}(W_{\bar{\imath}})}{\text{minimize}} \quad & \lambda_{\bar{\imath}}\|W_{\bar{\imath}}\|_1 + \sum_{\imath=1}^{\aleph} \lambda_\imath \|W_\imath\|_F + \frac{\lambda_e}{2}\|E\|_F^2 \\ \textit{Subject to} \quad \Theta \;&=\; \mathscr{A}_{\bar{\imath}}(W_{\bar{\imath}}) + \mathscr{A}_{\bar{\imath}}(W_{\bar{\imath}})^T + \sum_{\imath=1}^{\aleph} \mathscr{A}_\imath(W_\imath) + \mathscr{A}_\imath(W_\imath)^T + E, \end{aligned}$$

*where $\lambda_{\bar{\imath}}, \{\lambda_\imath\}_{\imath=1}^{\aleph}$ and $\lambda_e$ are non-negative regularization constants; $E$ is an unstructured noise matrix; $\|.\|_1$ denotes the $\ell_1$ norm or the sum of the absolute values of the matrix elements; and $\|.\|_F$ the Frobenius norm.*

**Remark 3** *Note that $\frac{\lambda_e}{2}\|E\|_F^2$ denotes a least squares loss function on the data fitting terms. The advantage of using $\frac{\lambda_e}{2}\|E\|_F^2$ is that we can apply a convergent multi-block ADMM to solve the problem of estimating a multi-structure graphical model where one seeks to decompose the matrix $\Theta$ into selected symmetric structured matrices. The subproblem for $E$ has a closed-form solution (see, Section 3 for more details).*

The overlap norm proposed by Tan et al. [49] promotes matrices that can be expressed as a union of few rows and the corresponding columns (i.e. hub nodes). However, $\Psi^{\mathscr{G}}$ is a new symmetric (and significantly more general) variant of the overlap norm that promotes matrices that can be expressed as the sum of symmetric structured matrices. Similar to [49], in order to recover all components of the matrix $\Theta$, $\Psi^{\mathscr{G}}$ needs a *priori* knowledge of its structures (e.g. size and location). We next introduce a new norm which simultaneously encourages different structures in $\Theta$, without requiring *a priori* knowledge of overlapping groups.

**Definition 4** *Let $\Theta$ be a $p \times p$ symmetric matrix containing the parameters of interest. The symmetric sparse structured overlap norm for a set of groups, $\mathscr{G}$ is given by,*

$$\begin{aligned} \Omega^{\mathscr{G}}(\Theta) := \underset{\Theta, Z_1, \ldots, Z_n,\ E}{\text{minimize}} \quad & \lambda_1 \quad \|Z_1 - \text{diag}(Z_1)\|_1 + \sum_{i=2}^{n} \Big( \hat{\lambda}_i \|Z_i - \text{diag}(Z_i)\|_1 \\ & + \quad \lambda_i \sum_{j=1}^{l} \|(Z_i - \text{diag}(Z_i))_j\|_F \Big) + \frac{\lambda_e}{2}\|E\|_F^2 \\ \textit{Subject to} \quad \Theta \;&=\; \sum_{i=1}^{n} Z_i + Z_i^T + E, \end{aligned} \tag{1}$$

*where $(Z_i)_j = W_i$ for $i = 2, \ldots, n$ and $j = 1, \ldots, l$ (see, Figure 2 for two examples of the structured matrix $Z_i$); $\{\hat{\lambda}_i\}_{i=1}^n$ and $\{\lambda_i\}_{i=1}^n$ are nonnegative regularization constants.*

**Remark 5** *Note that, in many instances, further refinement can be beneficial. While nonzero components may be clustered into groups, the nonzero groups may also be sparse. This goal can be achieved by the above formulation when $\{\hat{\lambda}_i\}_{i=1}^n$ are positive constants. Moreover, when $\{\hat{\lambda}_i\}_{i=1}^n \to \infty$ or $\{\lambda_i\}_{i=2}^n \to \infty$, then (1) reduces to $\ell_1$ norm. In this paper, we take Frobenius norm , which leads to estimation of a network containing dense subgraphs. Other values of norm such as $\infty$ are also possible.*

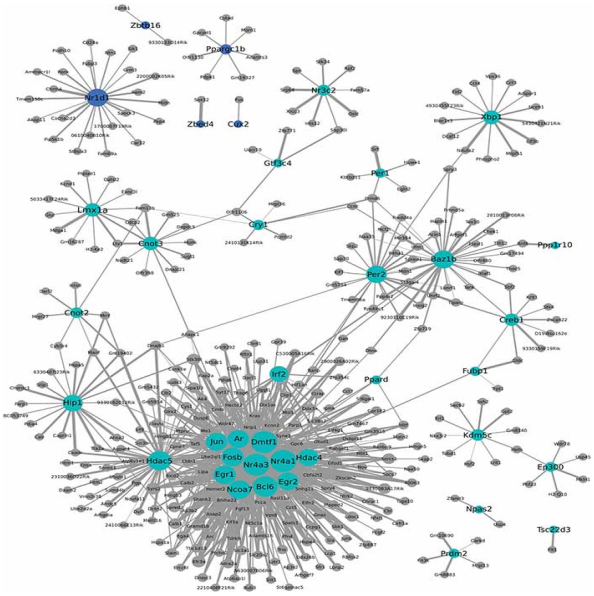

(a) Postpartum NAC Gene Network [54].

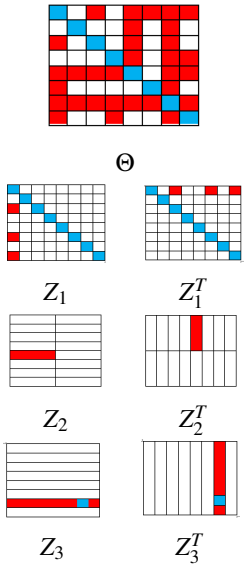


(b) An example of matrix partitioning for network in (a).

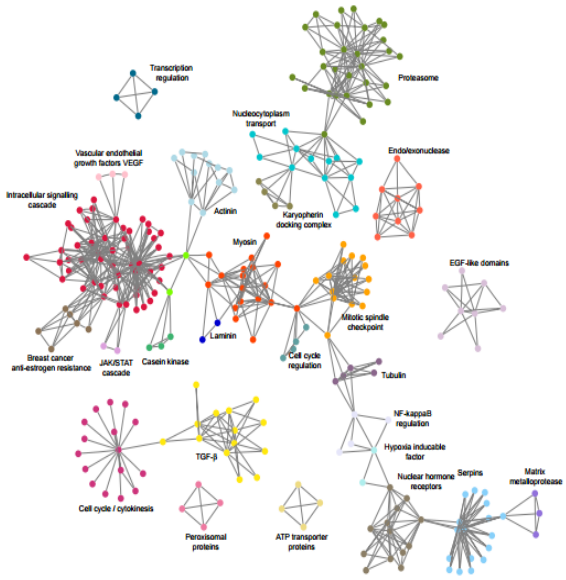


(c) The interactions between proteins in cancerous cells of a rat [28].

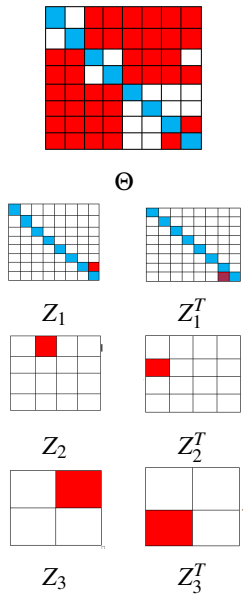


An example of matrix partitioning for network in (c).

Figure 2: The figure illustrates that block partition in structured matrices could be set based on a desire for interpretability of the resulting estimate. (a) and (c). Examples of structured gene networks. (b) and (d). Examples of proper structured matrices for network in (a) and (c), respectively. Blue elements are diagonal, white elements are zero and colored elements are non-zero partitions of the inverse covariance or covariance matrix $\Theta$. The structured penalty function (1) is then applied to each block in matrices $\{Z_i\}_{i=1}^n$.

We next use the symmetric sparse structured overlap norm as a regularizer for maximum likelihood estimation of widely-used probabilistic graphical models: (i) members of the Markov Random Field family -the Gaussian graphical model, the Gaussian graphical model with latent variables and the binary Ising model- and (ii) the Gaussian covariance graph model. For the sake of completeness, we provide a complete, but succinct description of the corresponding models and the proposed regularization.

## 2.1 Structured Gaussian Graphical Models

Let $X$ be a date matrix consisting of p–dimensional samples from a zero mean Gaussian distribution,

$$x_1,\ldots,x_m \overset{\text{i.i.d.}}{\sim} \mathscr{N}(0,\Sigma).$$

In order to obtain a sparse and interpretable estimate of the precision matrix $\Sigma^{-1}$ that captures conditional dependence relationships, many authors have considered the well-known *graphical lasso* problem [17, 46]

$$\underset{\Theta_1\in\mathscr{S}}{\text{minimize}} \quad \text{trace}(\hat{\Sigma}\Theta_1) - \log\det\Theta_1 + \lambda\left\|\Theta_1\right\|_1, \tag{2}$$

where $\Theta_1$ is a $p\times p$ symmetric matrix containing the parameters of interest; $\hat{\Sigma}$ is the empirical covariance matrix; $\mathscr{S}$ is the set of $p\times p$ symmetric positive definite matrices; and $\lambda$ is a non-negative tuning parameter.

As is well known, the norm penalty in (2) encourages zeros (sparsity) in the solution. However, in many biological and social network applications there are often more structures than just sparsity. Using the proposed norm, we define the following objective function for the problem at hand:

$$\begin{aligned} \underset{\Theta_1,Z_1,\ldots,Z_n\in\mathscr{S},\, E}{\text{minimize}} \quad & \text{trace}(\hat{\Sigma}\Theta_1) - \log\det\Theta_1 + \Omega^{\mathscr{G}}(\Theta_1), \\ \text{Subject to} \quad \Theta_1 \;&=\; \sum_{i=1}^{n} Z_i + Z_i^T + E. \end{aligned} \tag{3}$$

where $\Theta_1$ is the estimate of the precision matrix $\Sigma^{-1}$ and $\Omega^{\mathscr{G}}(\Theta_1)$ is the symmetric sparse structured overlap norm defined in (1).

Formulation (3) allows us to obtain a more accurate and compact graph estimation than conventional methods whenever the graph exhibits multiple structures. Moreover, our formulation does not require *a priori* knowledge of the underlying network structure (i.e. which nodes in the network form densely connected subgraphs (see Figure 3)). In Figure 3, the performance of our proposed approach is illustrated on three simulated data sets exhibiting multi-structure (subfigures (3c), (3f) and (3i)); it can be seen that the proposed structured graphical lasso (subfigures (3b), (4d) and (3h)) can recover the network structure much better than the popular graphical lasso based estimator [17](subfigures (3a), (3d) and (3g)).

## 2.2 Structured Binary Network

Another popular model, suitable for binary or categorical data, is the Ising one [27]. It is assumed that observations $x_1,\ldots,x_m$ are independent and identically distributed from

$$f(x,\Theta_2) = \frac{1}{\mathbb{W}(\Theta_2)}\exp\Big(\sum_{j=1}^{p}\theta_{jj}x_j + \sum_{1\le j<j'\le p}\theta_{jj'}x_jx_{j'}\Big), \tag{4}$$

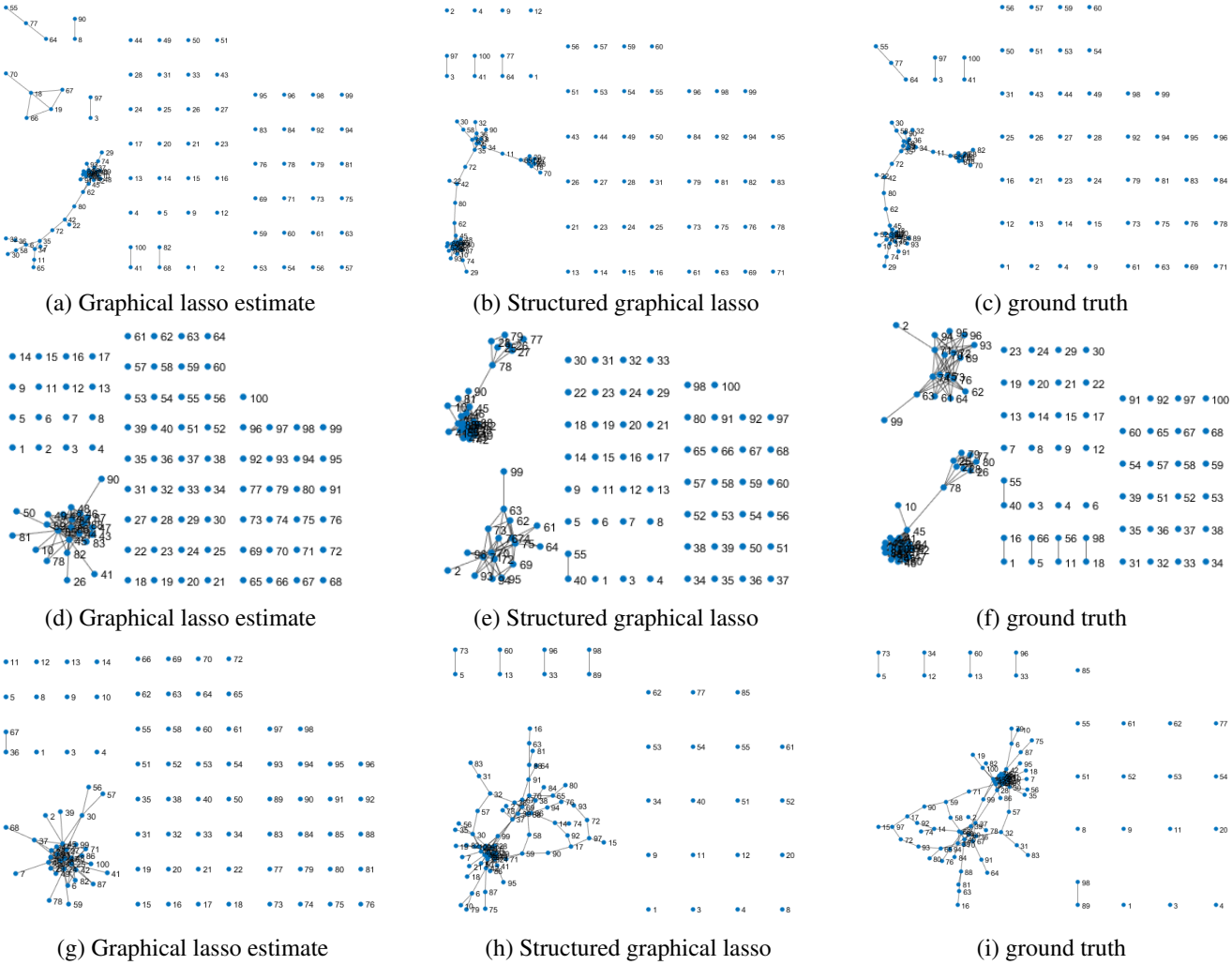

(a) Graphical lasso estimate (b) Structured graphical lasso (c) ground truth

(d) Graphical lasso estimate (e) Structured graphical lasso (f) ground truth

(g) Graphical lasso estimate (h) Structured graphical lasso (i) ground truth

Figure 3: Estimates from the structured graphical lasso proposed on three examples of Gaussian graphical models comprising of $p = 100$ nodes and: (3b) two structured matrices in (3); (4d) three structured matrices; (3h) four structured matrices.

where $\mathbb{W}(\Theta_2)$ is the partition function, which ensures that the density sums to one. Here, $\Theta_2$ is a $p \times p$ symmetric matrix that specifies the network structure: $\theta_{jj'} = 0$ implies that the $j$-th and $j'$-th variables are conditionally independent given the remaining ones.

Several papers proposing estimation procedures for this model have been published. Lee et al. in [30] considered maximizing an $\ell_1$-penalized log-likelihood for this model. Due to the difficulty in computing the log-likelihood with the computationally expensive partition function, several authors have considered alternative approaches. For instance, Ravikumar et al. [43] proposed a neighborhood selection approach. The proposal of Ravikumar et al. involves solving $p$ logistic regressions separately (one for each node), and hence, the estimated parameter matrix is not symmetric. In contrast, several authors considered maximizing an $\ell_1$-penalized pseudo-likelihood with a symmetric constraint on $\Theta_2$ (see, [21, 20]). Under the model (4), the log-pseudo-likelihood for $m$ observations takes

the form

$$\sum_{j=1}^{p}\sum_{j'=1}^{p}\theta_{jj'}(X^TX)_{jj'}-\sum_{i=1}^{m}\sum_{j=1}^{p}\log\Big(1+\exp\big(\theta_{jj}+\sum_{j'\neq j}\theta_{jj'}x_{ij'}\big)\Big). \tag{5}$$

We propose instead to impose the structured penalty function on $\Theta_2$ in (5) in order to estimate a binary network with multiple structures. This leads to the optimization problem

$$\begin{aligned}\underset{\Theta_2,Z_1,\ldots,Z_n\in\mathscr{S},\,E}{\text{minimize}} \quad & \sum_{j=1}^{p}\sum_{j'=1}^{p}\theta_{jj'}(X^TX)_{jj'}-\sum_{i=1}^{m}\sum_{j=1}^{p}\log\Big(1+\exp[\theta_{jj}+\sum_{j'\neq j}\theta_{jj'}x_{ij'}]\Big)+\Omega^{\mathscr{G}}(\Theta_2),\\ \text{Subject to} \quad & \Theta_2=\sum_{i=1}^{n}Z_i+Z_i^T+E.\end{aligned} \tag{6}$$

where $\Theta_2$ is the estimate of the precision matrix $\Sigma^{-1}$ and $\Omega^{\mathscr{G}}(\Theta_2)$ is the symmetric sparse strucuterd overlap norm as defined in (1).

### 2.3 Structured Gaussian Covariance Graphical Models

Next, we consider estimation of a covariance matrix under the assumption that $x_1,\ldots,x_m \overset{\text{i.i.d.}}{\sim} \mathscr{N}(0,\Sigma)$; this is of interest because the sparsity pattern of $\Sigma$ specifies the structure of the marginal independence graph [13, 14]. Let $\Theta_3$ be a $p\times p$ be a symmetric matrix containing the parameters of interest. Xue et al. in [52], proposed to estimate the positive definite covariance matrix, $\Sigma$ using

$$\underset{\Theta_3\in\mathscr{S}}{\text{minimize}}\left\{\frac{1}{2}\|\Theta_3-\hat{\Sigma}\|_{S_2}^2+\lambda\|\Theta_2\|_1\right\}, \tag{7}$$

where $\hat{\Sigma}$ is the empirical covariance matrix, $\mathscr{S}=\{\Theta_3:\Theta_3\succeq\varepsilon I \text{ and } \Theta_3=\Theta_3^T\}$, and $\varepsilon$ is a small positive constant. We extend (7) to accommodate structures of the covariance graph by imposing the symmetric sparse structured overlap norm on $\Theta_3$. This results in the following optimization problem:

$$\begin{aligned}\underset{\Theta_3,Z_1,\ldots,Z_n\in\mathscr{S},\,E}{\text{minimize}} \quad & \frac{1}{2}\|\Theta_2-\hat{\Sigma}\|_{S_2}^2+\Omega^{\mathscr{G}}(\Theta_3),\\ \text{Subject to} \quad \Theta_3 \quad = \quad & \sum_{i=1}^{n}Z_i+Z_i^T+E.\end{aligned} \tag{8}$$

where $\Theta_3$ is the estimate of the covariance matrix and $\Omega^{\mathscr{G}}(\Theta_3)$ is the symmetric sparse structured overlap norm as defined in (1).

### 2.4 Structured Gaussian Graphical Models with latent variables

In many applications throughout science and engineering, it is often the case that some relevant variables are not observed. For the Gaussian Graphical model, Chandrasekaran et al. [7] proposed a convex optimization problem to estimate it in the presence of latent variables. Their objective function is given next:

$$\begin{aligned}\underset{\Theta_4,Z_1,Z_2\in\mathscr{S}}{\text{minimize}} \quad & \langle\Theta_4,\Sigma_O\rangle-\log\det\Theta_4+\alpha\|Z_1\|_1+\beta\,\text{trace}(Z_{n+1})+\mathbb{1}_{Z_{n+1}\succeq 0},\\ \text{subject to} \quad & \Theta_4=Z_1-Z_{n+1},\end{aligned} \tag{9}$$

where $\Sigma_O$ is the sample covariance matrix of the observed variables; $\alpha$ and $\beta$ are positive constants; and the indicator function $\mathbb{1}_{Z_{n+1}\succeq 0}$ is defined as

$$\mathbb{1}_{Z_{n+1}\succeq 0} := \begin{cases} 0, & \text{if } Z_{n+1} \succeq 0, \\ +\infty, & \text{otherwise.} \end{cases}$$

This convex optimization problem aims to estimate an inverse covariance matrix that can be decomposed into a sparse matrix $Z_1$ minus a low-rank matrix $Z_{n+1}$ based on high-dimensional data.

We now extend the symmetric sparse structured overlap norm to solve the latent variable graphical model selection. Problem (9) can be rewritten in the following equivalent form by introducing new variables $\{Z_i\}_{i=2}^n$:

$$\begin{aligned} \underset{\Theta_4, Z_1, \ldots, Z_n \in \mathscr{S},\ E}{\text{minimize}} \quad & \langle \Theta_4, \hat{\Sigma}_Y \rangle - \log\det\Theta_4 + \Omega^{\mathscr{G}}(\Theta_4) + \lambda_{n+1}\,\text{trace}(Z_{n+1}) + \mathbb{1}_{Z_{n+1}\succeq 0} \\ \text{Subject to} \quad & \Theta_4 = \sum_{i=1}^{n} Z_i + Z_i^T - Z_{n+1} + E. \end{aligned} \tag{10}$$

where $\Theta_4$ is the estimate of the precision matrix $\Sigma^{-1}$ and $\Omega^{\mathscr{G}}(\Theta_4)$ is the symmetric sparse structured overlap norm as defined in (1).

Objective functions (3), (6), (8) and (10) involve separable convex functions and the constraint is simply linear, hence they are suitable for ADMM based algorithms. We next introduce a multi-block ADMM algorithm to solve these problems and establish its global convergence properties.

## 3 Multi-Block ADMM for Solving Structured Graphical Models

The alternating direction method of multipliers (ADMM) is widely used in solving structured convex optimization problems due to its superior practical performance[47, 5, 26, 35, 34, 48, 10, 22, 23]. On the theoretical side, Chen et al. [8] provided a counterexample showing that the multi-block ADMM may *fail to converge* without further conditions. Hence, many authors reformulate the problem of estimating a graphical model as a consensus problem [37, 49]. However, in the context of large-scale optimization problems, the consensus ADMM method becomes expensive due to its high memory requirements. Moreover, despite lack of convergence guarantees under standard convexity assumptions, it has been observed by many researchers that the unmodified multi-block ADMM often outperforms all its modified versions in practice [51, 48, 10].

Next, we present a convergent unmodified multi-block ADMM (without an upper bound on the penalty parameter) to solve convex problems (3), (6) and (8). The ADMM is constructed for an augmented Lagrangian function defined by

$$\begin{aligned} \mathscr{L}_\gamma(\Theta, Z_1, \ldots, Z_n, E; \Lambda) &= g(\Theta) + f_1(Z_1) + \cdots + f_n(Z_n) + \frac{\lambda_e}{2}\|E\|_F^2 \\ &- \langle \Lambda, \Theta - \sum_{i=1}^{n} Z_i - E \rangle + \frac{\gamma}{2}\|\Theta - \sum_{i=1}^{n} Z_i - E\|_F^2, \end{aligned} \tag{11}$$

where $\Lambda$ is the Lagrange multiplier, $\gamma$ a penalty parameter, $g(\Theta)$ the loss function of interest and

$$\begin{aligned} f_1(Z_1) &:= \lambda_1 \|Z_1 - diag(Z_1)\|_1, \\ f_i(Z_i) &:= \hat{\lambda}_i \|Z_i - \text{diag}(Z_i)\|_1 + \lambda_i \sum_{j=1}^{l} \|(Z_i - \text{diag}(Z_i))_j\|_F, \quad i = 2, \ldots, n. \end{aligned} \tag{12}$$

In a typical iteration of the ADMM for solving (11), the following updates are implemented:

$$\begin{aligned}
\Theta^{k+1} &:= \operatorname*{argmin}_{\Theta} \mathscr{L}_\gamma(\Theta, Z_1^k, \ldots Z_2^k, E^k; \Lambda^k),\\
Z_1^{k+1} &:= \operatorname*{argmin}_{Z_1} \mathscr{L}_\gamma(\Theta^{k+1}, Z_1, Z_2^k \ldots, Z_n^k, E^k; \Lambda^k),\\
&\vdots\\
Z_i^{k+1} &:= \operatorname*{argmin}_{Z_i} \mathscr{L}_\gamma(\Theta^{k+1}, Z_1^{k+1}, Z_2, Z_i^k, \ldots, Z_n^k, E^k; \Lambda^k),\\
&\vdots\\
Z_n^{k+1} &:= \operatorname*{argmin}_{Z_n} \mathscr{L}_\gamma(\Theta^{k+1}, Z_1^{k+1}, \ldots, Z_{n-1}^k, Z_n, E^k; \Lambda^k),\\
E^{k+1} &:= \operatorname*{argmin}_{E} \mathscr{L}_\gamma(\Theta^{k+1}, Z_1^{k+1}, Z_2^{k+1} \ldots, Z_n^{k+1}, E; \Lambda^k),\\
\Lambda^{k+1} &:= \Lambda^k - \gamma(\Theta^{k+1} - \sum_{i=1}^{n} Z_i^{k+1} - E^{k+1}).
\end{aligned} \tag{13}$$

The convex functions $\{f_i\}_{i=1}^n$ involved in the objective function (11) have easy to compute *proximal mappings* [5]:

$$\operatorname{prox}(f_i, \gamma, Z_i) := \operatorname*{argmin}_{Z_i} f_i(Z_i) + \frac{\gamma}{2}\|Z_i - C_i\|_F^2, \qquad i = 1, \ldots, n, \tag{14}$$

where

$$\begin{aligned}
C_1 &= \Theta^{k+1} - (Z_2^k + \cdots + Z_N^k + E^k + \frac{1}{\gamma}\Lambda^k)\\
C_i &= \Theta^{k+1} - (Z_1^{k+1} + \cdots + Z_{i-1}^{k+1} + Z_{i+1}^k + \ldots Z_n^k + E^k + \frac{1}{\gamma}\Lambda^k), \qquad i = 2, \ldots n-1.\\
C_n &= \Theta^{k+1} - (Z_1^{k+1} + \ldots Z_{n-1}^{k+1} + E^k + \frac{1}{\gamma}\Lambda^k).
\end{aligned} \tag{15}$$

It is well known that (14) has a closed-form solution that is given by the shrinkage operation:

$$\begin{aligned}
Z_1^{k+1} &= \operatorname{Shrink}\Big(C_1, \frac{\lambda_1}{\gamma}\Big),\\
Z_{i_j}^{k+1} &= \max\left(1 - \frac{\lambda_i}{\gamma\|\operatorname{Shrink}(C_{i_j}, \frac{\lambda_i}{\gamma})\|_F}, 0\right) \cdot \operatorname{Shrink}(C_{i_j}, \frac{\hat{\lambda}_i}{\gamma}), \quad \substack{i=2,\ldots n,\\ j=1,\ldots,l,}
\end{aligned} \tag{16}$$

where $\operatorname{Shrink}(\cdot,\cdot)$ in (16) denotes the soft-thresholds operator, applied element-wise to a matrix A [5]:

$$\operatorname{Shrink}(A_{ij}, b) := \operatorname{sign}(A_{ij}) \max\big(|A_{ij}| - b, 0\big) \qquad \substack{i=1,\ldots p,\\ j=1,\ldots,p,}$$

The discussions above suggest that the following unmodified ADMM for solving (11) would be an efficient algorithm.

**Algorithm 1** Multi-Block ADMM Algorithm for Solving (11).

1: **Initialize** The parameters:

(a) Primal variables $\Theta, Z_1, \ldots, Z_n, E$, to the $p \times p$ identity matrix.

(b) Dual variable $\Lambda$ to the $p \times p$ zero matrix.

(c) Constants $\lambda_e > 0$, $\tau > 0$ and $\gamma \geq \sqrt{2}\lambda_e$.

(d) Nonnegative regularization constants $\lambda_1, \ldots, \lambda_n$, $\hat{\lambda}_2, \ldots, \hat{\lambda}_n$.

2: **Iterate** Until the stopping criterion $\frac{\|\Theta^k - \Theta^{k-1}\|_F^2}{\|\Theta^{k-1}\|_F} \leq \tau$ is met:

(a) Update $\Theta$:

$$\Theta^{k+1} = \underset{\Theta \in \mathscr{S}}{\operatorname{argmin}} \left\{ g(\Theta) + \frac{\gamma}{2} \|\Theta - \left( Z_1^k + Z_2^k + \cdots + Z_n^k + E^k + \tfrac{1}{\gamma}\Lambda^k \right) \|_F^2 \right\}.$$

(b) Update $Z_i$:

i. $Z_1^{k+1} = \text{Shrink}\left(C_1, \frac{\lambda_1}{\gamma}\right)$, where $C_1$ is defined in (15).

ii. Set

$$Z_{i_j}^{k+1} = \max\left(1 - \frac{\lambda_i}{\gamma \|\text{Shrink}(C_{i_j}, \frac{\hat{\lambda}_i}{\gamma}\|_F}, 0\right) \cdot \text{Shrink}(C_{i_j}, \frac{\hat{\lambda}_i}{\gamma}), \qquad \begin{smallmatrix} i=2,\ldots n, \\ j=1,\ldots,l, \end{smallmatrix}$$

where $C_i$ is defined in (15).

(c) Update $E$:

$$E^{k+1} = \underset{E}{\operatorname{argmin}} \left\{ \frac{\lambda_e}{2} \|E\|_F^2 + \frac{\gamma}{2} \|\Theta^{k+1} - \left( Z_1^{k+1} + Z_2^{k+1} + \cdots + Z_n^{k+1} + E + \frac{1}{\gamma}\Lambda^k \right) \|_F^2 \right\}.$$

(d) Update $\Lambda$:

$$\Lambda^{k+1} = \Lambda^k - \gamma(\Theta^{k+1} - \textstyle\sum_{i=1}^n Z_i^{k+1} - E^{k+1}).$$

**Remark 6** *Note that in the case of solving problem* (10)*, one needs to add another block function* $f_{n+1}(Z_{n+1}) := \lambda_{n+1}\,\text{trace}(Z_{n+1}) + \mathbb{1}_{Z_{n+1} \succeq 0}$ *to the augmented Lagrangian function* (11) *and update* $\{C_i\}_{i=1}^n$*. In this case, the proximal mapping of* $f_{n+1}$ *is*

$$prox(f_{n+1}, \gamma, Z_{n+1}) := \underset{Z_{n+1}}{\operatorname{argmin}} f_{n+1}(Z_{n+1}) + \frac{\gamma}{2} \|Z_{n+1} - C_{n+1}\|_F^2, \tag{17}$$

*where* $C_{n+1} = -(\Theta^{k+1} - (\sum_{i=1}^n Z_i^{k+1} + E^k + \frac{1}{\gamma}\Lambda^k))$*. It is easy to verify that* (17) *has a closed-form solution*

$$Z_{n+1} = U\ \max(D - \frac{\lambda_{n+1}}{\gamma}, 0)\ U^T,$$

*where* $UDU^T$ *is the eigenvalue decomposition of* $C_{n+1}$*(see, [7, 37] for more details).*

### 3.1 Update for $\Theta$

In each iteration of Algorithm 1 the update for $\Theta$ depends on the form of the loss function $g(\Theta)$. We consider the following cases to update $\Theta$:

1. The update for $\Theta_1$ in Algorithm 1 (step 2(a)) can be obtained by minimizing

$$\text{trace}(\hat{\Sigma}\Theta_1) - \log\det\Theta_1 + \frac{\gamma}{2}\|\Theta_1 - (Z_1^k + Z_2^k + \cdots + Z_n^k + E^k + \frac{1}{\gamma}\Lambda^k)\|_F^2,$$

with respect to $\Theta_1$ (note that the constraint $\Theta_1 \in \mathscr{S}$ in (3) is treated as an implicit constraint, due to the domain of definition of the log det function). This can be shown to have the solution

$$\Theta_1 = \frac{1}{2}U\Big(D + \sqrt{D^2 + \frac{4}{\gamma}I}\Big)U^T,$$

where $UDU^T$ stands for the eigen-decomposition of $Z_1^k + Z_2^k + \cdots + Z_n^k + E^k + \frac{1}{\gamma}\Lambda^k - \frac{1}{\gamma}\hat{\Sigma}$.

2. Update for $\Theta_2$ in Step 2(a) of Algorithm 1 leads to the following optimization problem

$$\begin{aligned}\underset{\Theta_3 \in \mathscr{S}}{\text{minimize}}\ \Phi(\Theta_2) &= \sum_{j=1}^{p}\sum_{j'=1}^{p}\theta_{jj'}(X^TX)_{jj'} - \sum_{i=1}^{m}\sum_{j=1}^{p}\log\Big(1 + \exp[\theta_{jj} + \sum_{j'\neq j}\theta_{jj'}x_{ij'}]\Big) \\ &+ \frac{\gamma}{2}\|\Theta_2 - (Z_1^k + Z_2^k + \cdots + Z_n^k + E^k + \frac{1}{\gamma}\Lambda^k)\|_{S_2}^2. \end{aligned} \tag{18}$$

We use a novel non-monotone version of the Barzilai-Borwein method [3, 44, 15, 1] to solve (18). The details are given in Algorithm 2.

**Algorithm 2** Non-monotone Barzilai Borwein Method for Solving (18)

**Initialize** The parameters:

(a) $\Theta^0 = I$, $\Theta^1 = 2\Theta^0$, $\alpha^1 = 1$ and $t^0 = 10$.

(b) A positive sequence $\{\eta^t\}$ satisfying $\sum_{k=1}^{\infty}\eta^t = \eta < \infty$.

(c) Constants $\sigma > 0$, $\varepsilon > 0$, and $\nu \in (0,1)$.

**Iterate** Until the stopping criterion $\dfrac{\|\Theta^t - \Theta^{t-1}\|_{S_2}^2}{\|\Theta^{t-1}\|_{S_2}^2} \leq \varepsilon$ is met:

1. $\mathbb{G}^t = -\alpha^t\nabla\Phi(\Theta^t)$.
2. Set $\rho = 1$.
3. **If** $t > t^0$, **then**
   **While** $\|\Phi(\Theta^t + \rho^t\mathbb{G}^t)\|_{S_2} \leq \Phi(\Theta^t) + \eta^t - \sigma\rho^2{\alpha^t}^2\|\mathbb{G}^t\|_{S_2}^2$, **do**
   Set $\rho = \nu\rho$;
   **EndWhile**
   **EndIf**
4. Define $\rho^t = \rho$ and $\Theta^{t+1} = \Theta^t + \rho^t\mathbb{G}^t$.
5. Define $\alpha^{t+1} = \dfrac{\text{trace}\Big((\Theta^t - \Theta^{t+1})^T(\Theta^t - \Theta^{t+1})\Big)}{\text{trace}\Big((\nabla\Phi(\Theta^t) - \nabla\Phi(\Theta^{t+1}))^T(\Theta^t - \Theta^{t+1})\Big)}$

3. To update $\Theta_3$ in step 2(a), using (8), we have that

$$\begin{aligned}\underset{\Theta_3}{\text{minimize}}\ \frac{1}{2}\|\Theta_3-\hat{\Sigma}\|_{S_2}^2 \quad &+ \quad \frac{\gamma}{2}\|\Theta_3-\Big(Z_1^k+Z_2^k+\cdots+Z_n^k+E^k+\frac{1}{\gamma}\Lambda^k\Big)\|_{S_2}^2\\ &= \quad \Big(\frac{1}{1+\gamma}(\hat{\Sigma}+\gamma(Z_1^k+Z_2^k+\cdots+Z_n^k+E^k)+\Lambda^k)\Big)_+\end{aligned}$$

where $V_+ = U_\dagger D_+ U_\dagger$ such that

$$UDU = \begin{pmatrix} U_\dagger & U_\ddagger \end{pmatrix} \begin{pmatrix} D_+ & 0 \\ 0 & D_- \end{pmatrix} \begin{pmatrix} U_\dagger \\ U_\ddagger \end{pmatrix},$$

is the eigen-decomposition of the matrix $V$ , and $D_+$ and $D_-$ are the nonnegative and negative eigenvalues of $V$.

**Remark 7** *The complexity of Algorithm 1 is of the same order as the graphical lasso [17], the method in [49] for hub node discovery and the algorithm used for estimation of sparse covariance matrices introduced by [52]. Indeed, one can easily seen that with any decimation of matrices $\{Z_i\}_{i=1}^n$, the complexity of Algorithm 1 is equal to $O(p^3)$, which is the complexity of the eigen-decomposition for updating $\Theta$ in step 2(a).*

### 3.2 Convergence analysis

The next result establishes the global convergence of the standard multi-block ADMM for solving graphical model selection problems by using the Kurdyka- Lojasiewicz (KL) property of objective function (11).

**Theorem 8** *The sequence $U^k := (\Theta^k, Z_1^k, \ldots X_n^k, E^k, \Lambda^k)$ generated by Algorithm 1 from any starting point converges to a stationary point of the problem* (11).

*Proof.* A detailed exposition is given in Appendix 1.

## 4 Experimental Results

In this section, we present computational results of Algorithm 1, denoted by SGL, on both synthetic and real data to demonstrate the efficiency of the proposed method. The datasets, software code and results are available at `http://people.clas.ufl.edu/tarzanagh/`.

### 4.1 Experimental results on synthetic data

Before turning our attention to examining the real data sets, we evaluate the performance of SGL on ten synthetic problems, each with $p = 50$, 100, 500 and 1000 variables. The network structure in these problems corresponds to an Erdős-Rényi model graph, a nearest neighbor graph and a scale-free random graph, respectively. The CONTEST [1] package is used to generate the synthetic graphs, and the UGM [2] package to implement Gibbs sampling from the Ising Model. Based on the generated graph topologies, we consider the following set-ups for generating synthetic data sets:

[1] CONTEST is available at `http://www.mathstat.strath.ac.uk/outreach/contest/`

[2] UGM is available at `http://www.di.ens.fr/~mschmidt/Software/UGM.html`

I. **Gaussian graphical models**:
For a given number of variables $p$, we first create a symmetric matrix $E \in \mathbb{R}^{p\times p}$ by using CONTEST in a MATLAB environment. Given matrix $E$, we set $\Sigma^{-1}$ equal to $E + (0.1 - \bar{\Lambda}_{\min}(E))\, I$, where $\bar{\Lambda}_{\min}(E)$ is the smallest eigenvalue of $E$ and $I$ denotes the identity matrix. We then draw $N = 5p$ i.i.d. vectors $x_1, \ldots, x_m$ from the gasserian distribution $\mathcal{N}(0, \Sigma)$ by using the *mvnrnd* function in MATLAB, and then compute a sample covariance matrix of the variables.

II. **Gaussian covariance graphical models**:
The matrix $E \in \mathbb{R}^{p\times p}$ was generated as described in I. We set $\Sigma$ equal to $E + (0.1 - \bar{\Lambda}_{\min}(E))\, I$, where $\bar{\Lambda}_{\min}(E)$ is the smallest eigenvalue of $E$ and $I$ denotes the identity matrix. We then drew $N = 5p$ i.i.d. vectors $x_1, \ldots, x_m$ from the Gaussian distribution $\mathcal{N}(0, \Sigma)$ by using the *mvnrnd* function in MATLAB.

III. **Gaussian graphical models with latent variables:**
For a given number of variables $p$, we first create a matrix $\Sigma^{-1} \in \mathbb{R}^{(p+r)\times(p+r)}$ by using CONTEST as described in (I). We then choose the sub-matrix $\Theta_O = \Sigma^{-1}(1:p, 1:p)$ as the ground truth matrix of the matrix $\Theta_3$ and chose

$$\Theta_U \quad = \quad \Sigma^{-1}(1:p,\ p+1:p+r)\big(\Sigma^{-1}(p+1:p+r,\ p+r:p+r)\big)^{-1}\Sigma^{-1}(p+1:p+r,\ 1:p)$$

as the ground truth matrix of the low rank matrix $U$. We then draw $N = 5p$ i.i.d. vectors $x_1, \ldots, x_m$ from the Gaussian distribution $\mathcal{N}(0, (\Theta_O - \Theta_U)^{-1})$, and compute the sample covariance matrix of the variables $\Sigma_O$.

IV. **The Binary Network**:
To generate the parameter matrix $\Sigma$, we create an adjacency matrix as in Set-up (I) by using CONTEST. Then, each of $N = 5p$ observations is generated through Gibbs sampling. We take the first 100000 iterations as our burn-in period, and then collect observations, so that they are nearly independent.

We compare SGL to three sets of competitors:

- **CovSel**, designed to estimate a sparse Gaussian graphical model [17];
- **PGADM**, designed to learn a Gaussian graphical model with some latent nodes [37];
- **Pseudo-Exact**, designed to learn a binary Ising graphical model [25];

All the algorithms have been implemented in MATLAB 7.10.0 environment on a PC with CPU 2.0 GHz and 2Gb RAM memory. All the algorithms are being terminated either when

$$\frac{\|\Theta^k - \Theta^{k-1}\|_F^2}{\|\Theta^{k-1}\|_F^2} \leq \tau,$$

or the number of iterations and CPU times exceed 1,000 and 10 minutes, respectively. We set the parameters of the considered algorithms as follows:

$$\gamma = 2,\ \tau = 1e-5, \hat{\lambda}_1 = 0.1,\ \hat{\lambda}_i = 2\hat{\lambda}_1 \quad \text{for} \quad i = 2, 3, \ldots, n.$$

The penalty parameters $\{\lambda_i\}$ play an important rule for the convex decomposition to be successful [49, 53, **?**]. To select the regularization parameters $\lambda_i$, we propose the following adaptive formula

$$\lambda_i \sim \kappa\sqrt{log(\frac{p+\mathbb{S}_{ij}}{m})} \tag{19}$$

where $m$ is the sample size; $\kappa \in (0,1)$ and $\mathbb{S}_{ij}$ is the size of each block $Z_{ij}$.

We found that in practice the computation cost for computing the symmetric sparse structured overlap norm increases with the size of structured matrices. Therefore, we use a limited memory version of our symmetric sparse structured overlap norm in our experimental results. Block sizes in Figure 2 could be set based on a desire for interpretability of the resulting estimates. In this section, we choose four structured matrices with blocks $b_1 = [1,1]$ and $b_n = 2b_{n-1}$ for $n = 2,3,4$ (see, Figure 2). We define the following two performance measures, as suggested in [49]:

- Number of correctly estimated edges, $n_e$ :

$$\sum_{j<j'} \left( 1_{\{|\hat{\Theta}|>1e-4 \text{ and } |\Theta_{jj'}|\neq 0\}} \right).$$

- Sum of squared errors, $s_e$:

$$\sum_{j<j'} \left( |\hat{\Theta}_{jj'} - \Theta_{jj'}| \right)^2.$$

We have utilized the advantages of performance profile as proposed in [12] to display the efficiency of the algorithms considered, in terms of $n_e$ and $s_e$. As stated in [12], this profile provides a wealth of information such as solver efficiency, robustness and probability of success in compact form and eliminates the influence of a small number of problems on the evaluating process and the sensitivity of results associated with the ranking of solvers. Indeed, the performance profile plots the fraction of problem instances for which any given method is within a factor of the best solver. The horizontal axis of the figure gives the percentage of the test problems for which a method is efficient, while the vertical axis gives the percentage of the test problems that were successfully solved by each method (robustness). The performance profiles of the considered algorithms in log 2 scale are depicted in Figure 4. We compare SGL to three selected competitors for obtaining a sparse estimate of $\Theta$. Figure 4 provide performance profile of the considered algorithms for estimation of graphical models in terms of number of correctly estimated edges and sum of squared errors for the results of Tables 1 and 2 (provided in an appendix), respectively. The left and right figures are, respectively, drawn in terms of $n_e$ and $s_e$. From Figure 4, it can easily be seen that the proposed method works very well, since it solves all test problems without exhibiting any failure. Moreover, as it is clear from Figure 4, the SGL algorithm is the best algorithm among the considered algorithms, as it solves more than 80 % of the test problems in the maximum number of $n_e$ and minimum value of $s_e$. Furthermore, the performance index of SGL grows up rapidly in comparison with the other considered algorithms. The latter implies that whenever SGL is not the best algorithm, its performance index is close to the index of the best algorithm.

## 4.2 Experiments on structured data sets

In this section, we present numerical results on structured data sets to demonstrate the efficiency of SGL method. We investigate the behavior of SGL for a fixed value of $p = 100$. We set $b_1 = [1,1]$ and $b_n = 2 \cdot b_{n-1}$ for $n = 2,3,4$ (see, Figure 2). Results provided in Appendix A.2 indicate the efficiency of algorithm 1 on structured data sets. These results also show how the structure of the network returned by the two algorithms changes with growing $m$ (note that $\lambda_i$ and $\hat{\lambda}_i$ are kept fixed for each value of $m$).

## 4.3 Application to real data sets

### 4.3.1 US House voting data set

We applied the SGL method to describe the relationships amongst House Representatives in the U.S. Congress during the 2005-2006 period (109th Congress). The variables correspond to the 435 representatives, and the observations to the 1210 votes that the House deliberated and voted on during that period, which include bills, resolutions, motions, debates and roll call votes. The assumption of our model is that bills are i.i.d. sample from the same underlying Ising model. The votes are recorded as "yes" (encoded as "1") and "no" (encoded as "0"). Missing observations were replaced with the majority vote of the House members party on that particular vote. In order to detect multi-scale structure, we choose six symmetric structured matrices with block sizes $b_1 = [1,1]$, $b_2 = 10 \cdot b_1$ and $b_n = nb_2$ for $n = 2,\ldots,5$ (see, Figure 2). The penalty parameter was chosen based on (19) with $\kappa = 0.1$.

Following Guo et. al [19], we used a bootstrap procedure with the proposed estimator to evaluate the confidence of the estimated edges. Specifically, we estimated the network for multiple bootstrap samples of the same size, and only retained the edges that appeared more that $\omega$ percent of the time. The goal of the analysis is to understand the type of relationships that existed amongst the House members in the 109th Congress. In particular, we wish to identify and interpret the presence of densely connected components, as well of sparse components. The heatmap of the adjacency matrix of the estimated network by using the SGL algorithm is depicted in Figure 5. It can be easily seen that there exist locally strong connected components in the network, a fact that the glasso algorithm [17] fails to recover (see, Figure 6).

The network representation of subgraphs, with a cut-off value of 0.6, is given in Figures 7, 8 and 9. We only plot the edges associated with the subgraphs to enhance the visual reading of densely correlated areas. An interesting result of applying the SGL algorithm on this data set is the clear separation between members of the Democratic and Republican parties, as expected (see, Figures 7, 8 and 9). Indeed, members of the two political parties are clearly separated by using the SGL algorithm. Moreover, voting relationships within the two parties exhibit a clustering structure, which a closer inspection of the votes and subsequent analysis showed was mainly driven.

Other interesting patterns emerging from the analysis is that the SGL algorithm recovers members of opposite parties as a sparse component in each subgraph (see, Figures 7, 8 and 9). For instance, Figure 8 shows that Republican members such as Simpson, Kirk and Hyde are sparsely connected in a clustered group of Democratic members. This is possibly due to the overall centrist record of Kirk and alignment of Hyde and Simpson on selected issues. Similarly, Figure 8 indicates that Democratic members Bishop, Hastings and Meek are approximately sparsely connected to a subgraph of Republican members. Bishop from Georgia has compiled a fairly conservative voting record. The same conclusion can be derived from Figure 8. Indeed, Figures 7, 8 and 9 reveals that there are strong positive associations between members of the same party and negative associations between members of opposite parties. Obviously, at the higher cutoff value the dependence structure between members of opposite parties becomes sparser.

Other patterns of interest include a strong dependence between members of two opposite parties in selected subgraphs when the members come from the same state, as is the case for New York state members Jerrold Nadler (D), Anthony D. Weiner (D), Ed Towns (D), Major Owens (D), Nydia Velzquez (D), Vito Fossella (R), Carolyn B. Maloney (D), Charles B. Rangel (D), Jos Serrano (D), Eliot L. Engel (D), Nita Lowey (D), Sue W. Kelly (R), John E. Sweeney (R), Michael R. McNulty (D), Maurice Hinchey (D), John M. McHugh (R), Sherwood Boehlert (R), Jim Walsh (R), Tom Reynolds (R), Brian Higgins (D) -see Figure 8. However, in this instance, there is also a cluster of positive associations between Democrats.

In summary, the SGL algorithm provides deeper insights into relationships between House members, going beyond the obvious separation according to their voting record into two parties.

#### 4.3.2 Analysis of a breast cancer data set

We applied SGL to a data set containing 800 gene expression measurements from large epithelial cells sampled from 255 patients with breast cancer. The goal is to capture regulatory interactions amongst the genes, as well as to identify genes that tend to have interactions with other genes in a group and hence act as master regulators, thus providing insights into the molecular circuitry of the disease. Figure 10 depicts the heatmap of the estimated adjacency matrix for the breast cancer data set.

As it is clear in Figure 10, $Z_2, \ldots, Z_5$ and $Z_6$ show that selected genes are densely connected, which is not the case when employing the the graphical lasso algorithm (see, Figure 11). Therefore, SGL can provide an intuitive explanation of the relationships among the genes in the breast cancer data set (see, Figure 12 and 13 for two examples). These genes connectivity in the tumor samples may indicate a relationship that is common to an important subset of cancers. Many other genes belong to this network, each indicating a potentially interesting interaction in cancer biology. We omit the full list of locally correlated genes in our estimated network and provide a complete list in the on-line supplementary materials available in the first author's homepage.

## 5 Conclusion

In this paper, a new structured norm minimization method for solving multi-structure graphical model selection problems is proposed. Using the new structured norm approach, we can efficiently and accurately recover the underlying network structure. Our method utilizes a class of sparse structured norms in order to achieve higher order accuracy in approximating the decomposition of the data matrix. We then proposed an ADMM algorithm solving the resulting optimization problem. The global convergence of the method is established without any upper bound on the penalty parameter. We applied the proposed methodology to a number of real and synthetic data sets that establish its overall usefulness and good performance.

## References


[1] D. Ataee Tarzanagh, M. R. Peyghami, and H. Mesgarani. A new nonmonotone trust region method for unconstrained optimization equipped by an efficient adaptive radius. *Optimization Methods and Software*, 29(4):819–836, 2014.

[2] A.-L. Barabási and R. Albert. Emergence of scaling in random networks. *science*, 286(5439):509–512, 1999.

[3] J. Barzilai and J. M. Borwein. Two-point step size gradient methods. *IMA Journal of Numerical Analysis*, 8(1):141–148, 1988.

[4] J. Bolte, S. Sabach, and M. Teboulle. Proximal alternating linearized minimization for nonconvex and nonsmooth problems. *Mathematical Programming*, 146(1-2):459–494, 2014.

[5] S. Boyd, N. Parikh, E. Chu, B. Peleato, and J. Eckstein. Distributed optimization and statistical learning via the alternating direction method of multipliers. *Foundations and Trends® in Machine Learning*, 3(1):1–122, 2011.

[6] T. Cai and W. Liu. Adaptive thresholding for sparse covariance matrix estimation. *Journal of the American Statistical Association*, 106(494):672–684, 2011.

[7] V. Chandrasekaran, P. A. Parrilo, and A. S. Willsky. Latent variable graphical model selection via convex optimization. In *Communication, Control, and Computing (Allerton), 2010 48th Annual Allerton Conference on*, pages 1610–1613. IEEE, 2010.

[8] C. Chen, B. He, Y. Ye, and X. Yuan. The direct extension of admm for multi-block convex minimization problems is not necessarily convergent. *Mathematical Programming*, 155(1-2):57–79, 2016.

[9] P. Danaher, P. Wang, and D. M. Witten. The joint graphical lasso for inverse covariance estimation across multiple classes. *Journal of the Royal Statistical Society: Series B (Statistical Methodology)*, 76(2):373–397, 2014.

[10] D. Davis and W. Yin. A three-operator splitting scheme and its optimization applications. *arXiv preprint arXiv:1504.01032*, 2015.

[11] A. Defazio and T. S. Caetano. A convex formulation for learning scale-free networks via submodular relaxation. In *Advances in Neural Information Processing Systems*, pages 1250–1258, 2012.

[12] E. D. Dolan and J. J. Moré. Benchmarking optimization software with performance profiles. *Mathematical programming*, 91(2):201–213, 2002.

[13] M. Drton and T. S. Richardson. A new algorithm for maximum likelihood estimation in gaussian graphical models for marginal independence. In *Proceedings of the Nineteenth conference on Uncertainty in Artificial Intelligence*, pages 184–191. Morgan Kaufmann Publishers Inc., 2002.

[14] M. Drton and T. S. Richardson. Graphical methods for efficient likelihood inference in gaussian covariance models. *Journal of Machine Learning Research*, 9(May):893–914, 2008.

[15] R. Fletcher. On the barzilai-borwein method. In *Optimization and control with applications*, pages 235–256. Springer, 2005.

[16] S. Fortunato. Community detection in graphs. *Physics reports*, 486(3):75–174, 2010.

[17] J. Friedman, T. Hastie, and R. Tibshirani. Sparse inverse covariance estimation with the graphical lasso. *Biostatistics*, 9(3):432–441, 2008.

[18] R. Guimera and L. A. N. Amaral. Functional cartography of complex metabolic networks. *Nature*, 433(7028):895–900, 2005.

[19] J. Guo, J. Cheng, E. Levina, G. Michailidis, and J. Zhu. Estimating heterogeneous graphical models for discrete data with an application to roll call voting. *The annals of applied statistics*, 9(2):821, 2015.

[20] J. Guo, E. Levina, G. Michailidis, and J. Zhu. Asymptotic properties of the joint neighborhood selection method for estimating categorical markov networks. *arXiv preprint math.PR/0000000*, 2011.

[21] J. Guo, E. Levina, G. Michailidis, and J. Zhu. Joint estimation of multiple graphical models. *Biometrika*, page asq060, 2011.

[22] D. Hajinezhad and M. Hong. Nonconvex alternating direction method of multipliers for distributed sparse principal component analysis. In *2015 IEEE Global Conference on Signal and Information Processing (GlobalSIP)*, pages 255–259. IEEE, 2015.

[23] D. Hajinezhad, M. Hong, T. Zhao, and Z. Wang. Nestt: A nonconvex primal-dual splitting method for distributed and stochastic optimization. *arXiv preprint arXiv:1605.07747*, 2016.

[24] A. Hero and B. Rajaratnam. Hub discovery in partial correlation graphs. *IEEE Transactions on Information Theory*, 58(9):6064–6078, 2012.

[25] H. Höfling and R. Tibshirani. Estimation of sparse binary pairwise markov networks using pseudo-likelihoods. *Journal of Machine Learning Research*, 10(Apr):883–906, 2009.

[26] M. Hong and Z.-Q. Luo. On the linear convergence of the alternating direction method of multipliers. *arXiv preprint arXiv:1208.3922*, 2012.

[27] E. Ising. Beitrag zur theorie des ferromagnetismus. *Zeitschrift für Physik A Hadrons and Nuclei*, 31(1):253–258, 1925.

[28] P. F. Jonsson, T. Cavanna, D. Zicha, and P. A. Bates. Cluster analysis of networks generated through homology: automatic identification of important protein communities involved in cancer metastasis. *BMC bioinformatics*, 7(1):1, 2006.

[29] N. E. Karoui. Operator norm consistent estimation of large-dimensional sparse covariance matrices. *The Annals of Statistics*, pages 2717–2756, 2008.

[30] S.-I. Lee, V. Ganapathi, and D. Koller. Efficient structure learning of markov networks using $l_1$-regularization. In *Advances in neural Information processing systems*, pages 817–824, 2006.

[31] A. C. Lewis, N. S. Jones, M. A. Porter, and C. M. Deane. The function of communities in protein interaction networks at multiple scales. *BMC systems biology*, 4(1):1, 2010.

[32] L. Li, D. Alderson, J. C. Doyle, and W. Willinger. Towards a theory of scale-free graphs: Definition, properties, and implications. *Internet Mathematics*, 2(4):431–523, 2005.

[33] F. Liljeros, C. R. Edling, L. A. N. Amaral, H. E. Stanley, and Y. Åberg. The web of human sexual contacts. *Nature*, 411(6840):907–908, 2001.

[34] T. Lin, S. Ma, and S. Zhang. Iteration complexity analysis of multi-block admm for a family of convex minimization without strong convexity. *Journal of Scientific Computing*, pages 1–30, 2015.

[35] T. Lin, S. Ma, and S. Zhang. On the global linear convergence of the admm with multiblock variables. *SIAM Journal on Optimization*, 25(3):1478–1497, 2015.

[36] Q. Liu and A. T. Ihler. Learning scale free networks by reweighted l1 regularization. In *AISTATS*, pages 40–48, 2011.

[37] S. Ma, L. Xue, and H. Zou. Alternating direction methods for latent variable gaussian graphical model selection. *Neural computation*, 25(8):2172–2198, 2013.

[38] J. Mairal, F. Bach, J. Ponce, and G. Sapiro. Online learning for matrix factorization and sparse coding. *Journal of Machine Learning Research*, 11(Jan):19–60, 2010.

[39] M. E. Newman. The structure of scientific collaboration networks. *Proceedings of the National Academy of Sciences*, 98(2):404–409, 2001.

[40] M. E. Newman. Communities, modules and large-scale structure in networks. *Nature Physics*, 8(1):25–31, 2012.

[41] M. E. Newman and M. Girvan. Finding and evaluating community structure in networks. *Physical review E*, 69(2):026113, 2004.

[42] G. Obozinski, L. Jacob, and J.-P. Vert. Group lasso with overlaps: the latent group lasso approach. *arXiv preprint arXiv:1110.0413*, 2011.

[43] P. Ravikumar, M. J. Wainwright, G. Raskutti, B. Yu, et al. High-dimensional covariance estimation by minimizing 1-penalized log-determinant divergence. *Electronic Journal of Statistics*, 5:935–980, 2011.

[44] M. Raydan. The barzilai and borwein gradient method for the large scale unconstrained minimization problem. *SIAM Journal on Optimization*, 7(1):26–33, 1997.

[45] G. Robins, P. Pattison, Y. Kalish, and D. Lusher. An introduction to exponential random graph (p*) models for social networks. *Social networks*, 29(2):173–191, 2007.

[46] A. J. Rothman, P. J. Bickel, E. Levina, J. Zhu, et al. Sparse permutation invariant covariance estimation. *Electronic Journal of Statistics*, 2:494–515, 2008.

[47] K. Scheinberg, S. Ma, and D. Goldfarb. Sparse inverse covariance selection via alternating linearization methods. In *Advances in neural information processing systems*, pages 2101–2109, 2010.

[48] D. Sun, K.-C. Toh, and L. Yang. A convergent 3-block semiproximal alternating direction method of multipliers for conic programming with 4-type constraints. *SIAM journal on Optimization*, 25(2):882–915, 2015.

[49] K. M. Tan, P. London, K. Mohan, S.-I. Lee, M. Fazel, and D. M. Witten. Learning graphical models with hubs. *Journal of Machine Learning Research*, 15(1):3297–3331, 2014.

[50] A. L. Traud, E. D. Kelsic, P. J. Mucha, and M. A. Porter. Comparing community structure to characteristics in online collegiate social networks. *SIAM review*, 53(3):526–543, 2011.

[51] X. Wang, M. Hong, S. Ma, and Z.-Q. Luo. Solving multiple-block separable convex minimization problems using two-block alternating direction method of multipliers. *arXiv preprint arXiv:1308.5294*, 2013.

[52] L. Xue, S. Ma, and H. Zou. Positive-definite $\ell_1$-penalized estimation of large covariance matrices. *Journal of the American Statistical Association*, 107(500):1480–1491, 2012.

[53] M. Yuan and Y. Lin. Model selection and estimation in the gaussian graphical model. *Biometrika*, 94(1):19–35, 2007.

[54] C. Zhao, B. E. Eisinger, T. M. Driessen, and S. C. Gammie. Addiction and reward-related genes show altered expression in the postpartum nucleus accumbens. *Frontiers in behavioral neuroscience*, 8, 2014.

# A Appendix

## A.1 Appendix A.

Before establishing the main result on global convergence of the proposed ADMM algorithm, we provide the necessary definitions used in the proofs (for more details see, [4]):

**Definition 9** *(Kurdyka- Lojasiewicz property).*
*The function $f$ is said to have the Kurdyka- Lojasiewicz (K-L) property at point $Z_0$, if there exist $c_1 > 0$, $c_2 > 0$ and $\phi \in \Gamma_{c_2}$ such that for all*

$$Z \in B(Z_0, c_1) \cap \{Z : f(Z_0) < f(Z) < f(Z_0) + c_2\},$$

*the following inequality holds*

$$\nabla\phi\big(f(Z) - f(Z_0)\big)\, dist\big(0, \partial f(Z)\big) \geq 1,$$

*where $\Gamma_{c_2}$ stands for the class of functions $\phi : [0, c_2] \to \mathbb{R}^+$ with the properties:*

*(i)* *$\phi$ is continuous on $[0, c_2)$;*

*(ii)* *$\phi$ is smooth concave on $(0, c_2)$;*

*(iii)* *$\phi(0) = 0$, $\nabla\phi(s) > 0$, $\forall\, s \in (0, c_2)$.*

**Definition 10** *(Semi-algebraic sets and functions).*

*(i)* *A subset $C \in \mathbb{R}^{n\times n}$ is semi-algebraic, if there exists a finite number of real polynomial functions $h_{ij}$, $s_{ij} : \mathbb{R}^{n\times n} \to \mathbb{R}$ such that*

$$C = \cup_{i=1}^{\bar{p}} \cap_{j=1}^{\bar{q}} \{Z \in \mathbb{R}^{n\times n} :\ g_{ij}(Z) = 0 \quad and \quad s_{ij}(Z) < 0\}.$$

*(ii) A function* $h : \mathbb{R}^{n\times n} \to (-\infty, +\infty]$ *is called semi-algebraic, if its graph*

$$\mathbb{G}(h) := \{(Z, y) \in \mathbb{R}^{n\times n+1} : h(Z) = y\},$$

*is a semi-algebraic set in* $R^{n\times n+1}$.

**Definition 11** *(Sub-analytic sets and functions).*

*(i) A subset* $C \in \mathbb{R}^{n\times n}$ *is sub-analytic, if there exists a finite number of real analytic functions* $h_{ij}$, $s_{ij} : \mathbb{R}^{n\times n} \to \mathbb{R}$ *such that*

$$C = \cup_{i=1}^{\bar{p}} \cap_{j=1}^{\bar{q}} \{Z \in \mathbb{R}^d : g_{ij}(Z) = 0 \quad \textit{and} \quad s_{ij}(Z) < 0\}.$$

*(ii) A function h:* $R^{n\times n} \to (-\infty, +\infty]$ *is called sub-analytic, if its graph*

$$\mathbb{G}(h) := \{(Z, y) \in \mathbb{R}^{n\times n+1} : h(Z) = y\}$$

*is a sub-analytic set in* $R^{n\times n+1}$.

It can be easily seen that both real analytic and semi-algebraic functions are sub-analytic. In general, the sum of two sub-analytic functions is not necessarily sub-analytic. However, it is easy to show that for two sub-analytic functions, if at least one function maps bounded sets to bounded sets, then their sum is also sub-analytic [4].

**Remark 12** *Each* $f_i$ *in* (12) *is a convex semi-algebraic function (see, example 5.3 in [4]), while the loss function* $g(\Theta)$ *in* (3), (6), (8) *and* (10) *is sub-analytic (even analytic). Since each function* $f_i$ *maps bounded sets to bounded sets, we can conclude that the augmented Lagrangian function*

$$\begin{aligned} \mathscr{L}_\gamma(\Theta, Z_1, \ldots, Z_n, E; \Lambda) &= g(\Theta) + f_1(Z_1) + \cdots + f_n(Z_n) + \frac{\lambda_e}{2}\|E\|_F^2 \\ &- \langle \Lambda, \Theta - \sum_{i=1}^{n} Z_i - E\rangle + \frac{\gamma}{2}\|\Theta - \sum_{i=1}^{n} Z_i - E\|_F^2, \end{aligned}$$

*which is the summation of sub-analytic functions is itself sub-analytic. All sub-analytic functions which are continuous over their domain satisfy a K-L inequality, as well as some, but not all, convex functions (see [4] for details and a counterexample). Therefore, the augmented Lagrangian function* $\mathscr{L}_\gamma$ *satisfies the K-L property.*

Next, we establish a series of lemmas used in the proof of Theorem 8.

**Lemma 13** *Let* $U^k := (\Theta^k, Z_1^k, \ldots, Z_n^k, E^k; \Lambda^k)$ *be a sequence generated by Algorithm 1, then there exists a positive constant* $\vartheta$ *such that*

$$\mathscr{L}_\gamma(U^{k+1}) \leq \mathscr{L}_\gamma(U^k) - \frac{\vartheta}{2}\Big(\|\Theta^k - \Theta^{k+1}\|_F + \sum_{i=1}^{n}\|Z_i^k - Z_i^{k+1}\|_F + \|E^k - E^{k+1}\|_F + \|\Lambda^k - \Lambda^{k+1}\|_F\Big).$$

*Proof.* Using the first-order optimality conditions for (11) and the convexity of $g(\Theta)$, we obtain

$$\begin{aligned}
0 &= \langle \Theta^k - \Theta^{k+1}, \nabla g(\Theta^{k+1}) - \Lambda^k + \gamma(\Theta^{k+1} - \sum_{i=1}^n Z_i^k - E^k)\rangle \\
&\leq g(\Theta^k) - g(\Theta^{k+1}) - \langle \Theta^k - \Theta^{k+1}, \Lambda^k\rangle + \gamma\langle \Theta^k - \Theta^{k+1}, \Theta^{k+1} - \sum_{i=1}^n Z_i^k - E^k\rangle \\
&= g(\Theta^k) - \langle \Theta^k, \Lambda^k\rangle + \frac{\gamma}{2}\sum_{i=1}^n \|\Theta^k - Z_i^k - E^k\|_F^2 - \frac{\gamma}{2}\|\Theta^k - \Theta^{k+1}\|_F^2 \\
&- \Big(g(\Theta^{k+1}) - \langle \Theta^{k+1}, \Lambda^k\rangle + \frac{\gamma}{2}\|\Theta^{k+1} - \sum_{i=1}^n Z_i^k - E^k\|_F^2\Big) \\
&= \mathscr{L}_\gamma(U^k) - \mathscr{L}_\gamma(\Theta^{k+1}, Z_1^k, \ldots, Z_n^k, E^k; \Lambda^k) - \frac{\gamma}{2}\|\Theta^k - \Theta^{k+1}\|_F^2, \qquad (20)
\end{aligned}$$

where the second equality follows from the fact that

$$(u_1 - u_2)^T(u_3 - u_1) = \frac{1}{2}\Big(\|u_2 - u_3\|_F^2 - \|u_1 - u_2\|_F^2 - \|u_1 - u_3\|_F^2\Big).$$

Similarly, we obtain that

$$\begin{aligned}
&\mathscr{L}_\gamma(\Theta^{k+1}, \ldots, Z_{i-1}^{k+1}, Z_i^k, \ldots, E^k; \Lambda^k) - \mathscr{L}_\gamma(\Theta^{k+1}, \ldots, Z_i^{k+1}, Z_{i+1}^k, \ldots, E^k; \Lambda^k) - \frac{\gamma}{2}\|Z_i^k - Z_i^{k+1}\|_F^2 \geq 0, \\
&\mathscr{L}_\gamma(\Theta^k, Z_1^{k+1}, \ldots, Z_n^{k+1}, E^k; \Lambda^k) - \mathscr{L}_\gamma(\Theta^{k+1}, Z_1^{k+1}, \ldots, Z_n^{k+1}, E^{k+1}; \Lambda^k) - \frac{\gamma}{2}\|E^k - E^{k+1}\|_F^2 \geq 0, \\
&\mathscr{L}_\gamma(\Theta^{k+1}, Z_1^{k+1}, \ldots, Z_n^{k+1}, E^{k+1}; \Lambda^k) - \mathscr{L}_\gamma(U^{k+1}) - \frac{\lambda_e^2}{\gamma}\|E^k - E^{k+1}\|_F^2 \geq 0, \qquad (21)
\end{aligned}$$

for $i = 1, \ldots, n$. Now, letting $\bar{\gamma} := \frac{\gamma^2 - 2\lambda_e^2}{\gamma(1+\lambda_e^2)}$, $\vartheta := \max(\bar{\gamma}, \gamma)$ and using (20), and (21), we get

$$\begin{aligned}
&\mathscr{L}_\gamma(U^k) - \mathscr{L}_\gamma(U^{k+1}) \geq \frac{\gamma}{2}\Big(\|\Theta^k - \Theta^{k+1}\|_F^2 + \sum_{i=1}^n \|Z_i^k - Z_i^{k+1}\|_F^2\Big) + \frac{\gamma^2 - 2\lambda_e^2}{2\gamma}\|E^k - E^{k+1}\|_F^2, \\
= \;& \frac{\gamma}{2}\Big(\|\Theta^k - \Theta^{k+1}\|_F^2 + \sum_{i=1}^n \|Z_i^k - Z_i^{k+1}\|_F^2\Big) + \frac{\bar{\gamma}}{2}\|E^k - E^{k+1}\|_F^2 + \frac{\lambda_e^2\bar{\gamma}}{2}\|E^k - E^{k+1}\|_F^2, \\
= \;& \frac{\gamma}{2}\Big(\|\Theta^k - \Theta^{k+1}\|_F^2 + \sum_{i=1}^n \|Z_i^k - Z_i^{k+1}\|_F^2\Big) + \frac{\bar{\gamma}}{2}\Big(\|E^k - E^{k+1}\|_F^2 + \|\Lambda^k - \Lambda^{k+1}\|_F^2\Big), \\
\geq \;& \frac{\vartheta}{2}\Big(\|\Theta^k - \Theta^{k+1}\|_F^2 + \sum_{i=1}^n \|Z_i^k - Z_i^{k+1}\|_F^2 + \|E^k - E^{k+1}\|_F^2 + \|\Lambda^k - \Lambda^{k+1}\|_F^2\Big).
\end{aligned}$$

□

**Lemma 14** *Let $U^k = (\Theta^k, Z_1^k, \ldots X_n^k, E^k, \Lambda^k)$ be a sequence generated by Algorithm 1. Then, there exists a subsequence $U^{k_s}$ of $\{U^k\}$, such that*

$$\lim_{s\to\infty} g(\Theta^{k_s}) = g(\Theta^*), \quad \lim_{s\to\infty} f_i(Z_i^{k_s}) = f_i(Z_i^*), \quad \lim_{s\to\infty} f_e(E_i^{k_s}) = f_e(E_i^*),$$

*where*

$$\lim_{s\to\infty} U^{k_s} = (\Theta^*, Z_1^*, \ldots, Z_n^*, E^*, \Lambda^*).$$

*Proof.* Using the quadratic function $f_e(E) = \frac{\lambda_e}{2}\|E\|_F^2$, we have that

$$\begin{aligned} f_e(E^{k+1} - (\Theta^{k+1} - \sum_{i=1}^{n} Z_i^{k+1} - E^{k+1})) &= \frac{\lambda_e}{2}\|E^{k+1} - (\Theta^{k+1} - \sum_{i=1}^{n} Z_i^{k+1} - E^{k+1})\|_F^2 \\ &= \frac{\lambda_e}{2}\|E^{k+1}\|^2 - \lambda_e\langle E^{k+1}, \Theta^{k+1} - \sum_{i=1}^{n} Z_i^{k+1} - E^{k+1}\rangle \\ &+ \frac{\lambda_e}{2}\|\Theta^{k+1} - \sum_{i=1}^{n} Z_i^{k+1} - E^{k+1}\|_F^2, \end{aligned} \tag{22}$$

Using (12) and (22), there exists $\underline{\mathscr{L}}$, such that

$$\begin{aligned} \mathscr{L}_\gamma(U^{k+1}) &= g(\Theta^{k+1}) + f_1(Z_1^{k+1}) + \ldots f_n(Z_n^{k+1}) + \frac{\lambda_e}{2}\|E^{k+1} - (\Theta^{k+1} - \sum_{i=1}^{n} Z_i^{k+1} - E^{k+1})\|_F^2 \\ &+ \frac{\gamma - \lambda_e}{2}\|\Theta^{k+1} - \sum_{i=1}^{n} Z_i^{k+1} - E^{k+1}\|_F^2 \geq \underline{g} + \underline{f_1} + \cdots + \underline{f_n} \geq \underline{\mathscr{L}}, \end{aligned} \tag{23}$$

since $g(\Theta^{k+1})$ and $f_i(Z_i^{k+1})(i = 1, \ldots, n)$ are all lower bounded. Now, using Lemma 13, we have that

$$\begin{aligned} \frac{\vartheta}{2}\sum_{k=0}^{K}\Big(\|\Theta^k - \Theta^{k+1}\|_F^2 + \sum_{i=1}^{n}\|Z_i^k - Z_i^{k+1}\|_F^2 &+ \|E^k - E^{k+1}\|_F^2 + \|\Lambda^k - \Lambda^{k+1}\|_F^2\Big) \\ &\leq \mathscr{L}_\gamma(U^0) - \underline{\mathscr{L}} \end{aligned} \tag{24}$$

Lemma 13 together with (23) shows that $\mathscr{L}_\gamma(U^k)$ converges to $\mathscr{L}_\gamma(U^*)$. Note that (23) and the coerciveness of $g(\Theta)$ and $f_i$ $(i = 1, \ldots, n)$ imply that $\{(\Theta^k, Z_1^k, \ldots, Z_n^k)\}$ is a bounded sequence. This together with the updating formula of $\Lambda^{k+1}$ and (24) yield the boundedness of $E^{k+1}$. Moreover, the fact that $\Lambda^k = \lambda_e E^k$, gives the boundedness of $\Lambda^k$, which implies that the entire sequence $\{U^k\}$ is a bounded one. Therefore, there exists a subsequence

$$U^{k_s} = (\Theta^{k_s}, Z_1^{k_s}, \ldots, Z_n^{k_s}, E^{k_s}; \Lambda^{k_s}), \qquad s = 0, 1, \ldots$$

such that $U^{k_s} \to U^*$ as $s \to \infty$.

Now, using the fact that $g(\Theta)$, $f_i(Z_i)$ $(i = 1, \ldots, n)$ and $f_e(E)$ are continuous functions, we have that

$$\lim_{s\to\infty} g(\Theta^{k_s}) = g(\Theta^*), \quad \lim_{s\to\infty} f_i(Z_i^{k_q}) = f_i(Z_i^*), \quad \lim_{s\to\infty} f_e(E_i^{k_q}) = f_e(E_i^*).$$

□

**Lemma 15** *Algorithm 1 either stops at a stationary point of the problem* (11) *or generates an infinite sequence* $\{U^k\}$*, so that any limit point of* $\{U^k\}$ *is a critical point of* $\mathscr{L}_\gamma(U^k)$ (11)*.*

*Proof.* From the definition of the augmented Lagrangian function in (11), we have that

$$\begin{aligned} &\nabla g(\Theta^{k+1}) - \Lambda^{k+1} + \gamma(\Theta^{k+1} - \sum_{i=1}^{n} Z_i^{k+1} - E^k) = \nabla_\Theta \mathscr{L}_\gamma(U^{k+1}), \\ &\partial f_i(Z_i^{k+1}) - \Lambda^{k+1} + \gamma(\Theta^{k+1} - \sum_{i=1}^{n} Z_i^{k+1} - E^{k+1}) = \partial_{Z_i}\mathscr{L}_\gamma(U^{k+1}), \quad i = 1, \ldots, n, \\ &\lambda_e E^{k+1} - \Lambda^{k+1} + \gamma(\Theta^{k+1} - \sum_{i=1}^{n} Z_i^{k+1} - E^{k+1}) = \nabla_E \mathscr{L}_\gamma(U^{k+1}), \\ &\gamma(E^{k+1} + \sum_{i=1}^{n} Z_i^{k+1} - \Theta^{k+1}) = \nabla_\Lambda \mathscr{L}_\gamma(U^{k+1}), \end{aligned} \tag{25}$$

Moreover, the updating formula of $\Lambda^{k+1}$ and (12) yields that

$$\begin{aligned}
&\nabla g(\Theta^{k+1}) - \Lambda^{k+1} = \gamma(\Theta^{k+1} - \Theta^k + \sum_{i=1}^{n} Z_i^k - Z_i^{k+1} + E^k - E^{k+1}) \\
&\partial f_1(Z_1^{k+1}) - \Lambda^{k+1} = \gamma(\sum_{i=2}^{n} Z_i^k - Z_i^{k+1} + E^k - E^{k+1}) \\
&\partial f_i(Z_i^{k+1}) - \Lambda^{k+1} = \gamma(\sum_{j=i+1}^{n} Z_j^k - Z_j^{k+1} + E^k - E^{k+1}) \quad i = 2, \ldots, n \\
&\lambda_e E^{k+1} - \Lambda^{k+1} = 0.
\end{aligned} \tag{26}$$

Combining (25), (26), and the updating formula of $\Lambda^{k+1}$, we have that

$$(\hbar_\Theta^{k+1}, \hbar_1^{k+1}, \ldots, \hbar_n^{k+1}, \hbar_E^{k+1}, \hbar_\Lambda^{k+1}) \in \partial \mathscr{L}_\gamma(U^{k+1}), \tag{27}$$

where

$$\begin{aligned}
&\hbar_\Theta^{k+1} := \Lambda^k - \Lambda^{k+1} + \gamma(\Theta^{k+1} - \Theta^k + \sum_{i=1}^{n} Z_i^k - Z_i^{k+1} + E^k - E^{k+1}), \\
&\hbar_{Z_i}^{k+1} := \Lambda^k - \Lambda^{k+1} + \gamma(\sum_{j=i+1}^{n} Z_i^k - Z_i^{k+1} + E^k - E^{k+1}), \quad i = 1, \ldots, n, \\
&\hbar_E^{k+1} := \Lambda^k - \Lambda^{k+1}, \\
&\hbar_\Lambda^{k+1} := \frac{1}{\gamma}(\Lambda^{k+1} - \Lambda^k),
\end{aligned} \tag{28}$$

Now, using (24), we obtain that

$$\lim_{k\to\infty} (\|\hbar_\Theta^{k+1}\|_F, \|\hbar_{Z_1}^{k+1}\|_F, \ldots, \|\hbar_{Z_n}^{k+1}\|_F, \|\hbar_E^{k+1}\|_F; \|R_\Lambda^{k+1}\|_F) = (0, \ldots, 0). \tag{29}$$

Suppose that Algorithm 1 does not stop at a stationary point. Using Lemma 14, there exists a subsequence $U^{k_s}$, such that $U^{k_s} \to U^*$ as $s \to \infty$. Using (27) and (29), we conclude that $(0, \ldots, 0) \in \partial \mathscr{L}_\gamma(U^*)$. □

**Proof of Theorem 8.** Lemmas 14 and 15 imply that $\{U^k\}$ is a bounded sequence and the set of limit points of $\{U^k\}$ starting from $U^0$ is non-empty, respectively. Moreover, Lemma 5 and Remark 5 of [4] imply that the set of limit points of $\{U^k\}$ starting from $U^0$ is compact. The remainder of the proof of this Theorem follows along similar lines to the proof of Theorem 1 in [4], by utilizing the K-L property of the problem (11) (see, Remark 12). □

## A.2 Appendix B

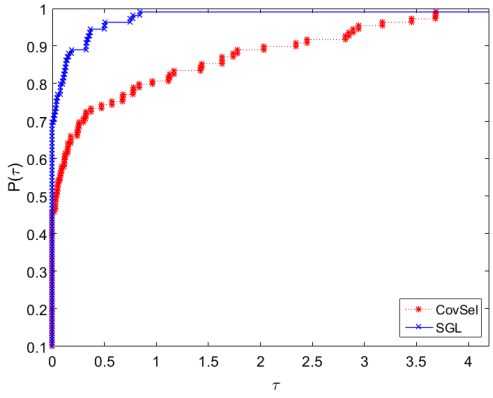


(a) Performance based on Num. Corr. Est. edges.

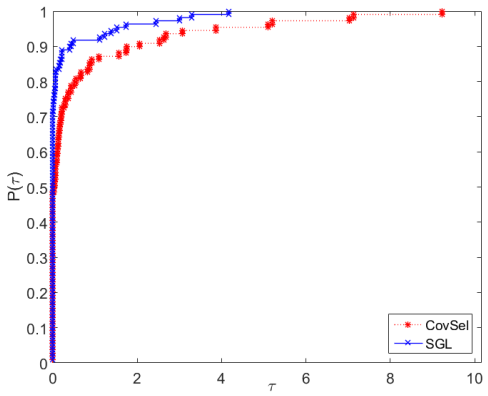


(b) Performance based on sum of squared errors

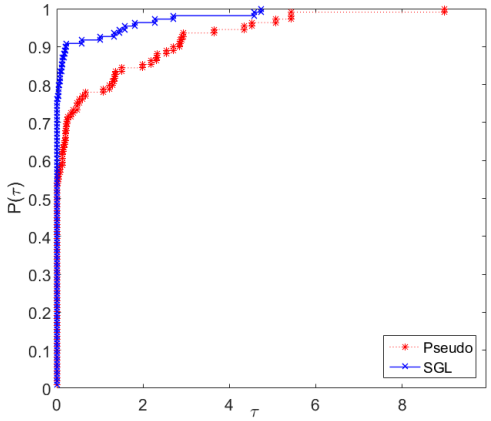


(c) Performance based on Num. Corr. Est. edges.

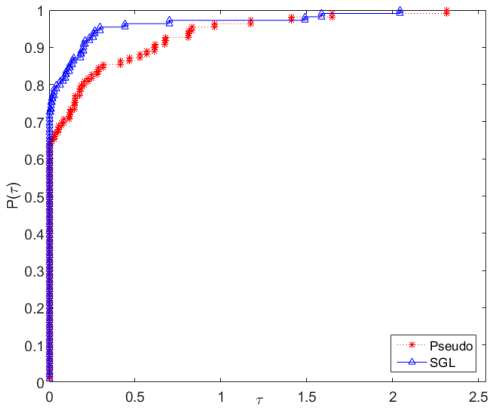


(d) Performance based on sum of squared errors

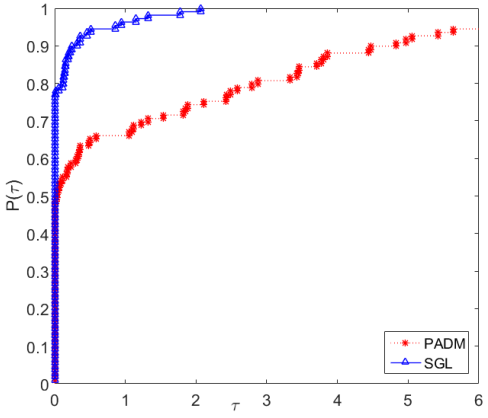


(e) Performance based on Num. Corr. Est. edges.

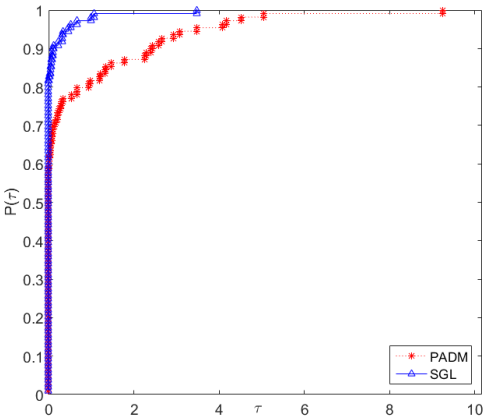


(f) Performance based on sum of squared errors

Figure 4: Performance profiles of CovSel, PGADM and Pseudo-Exact.

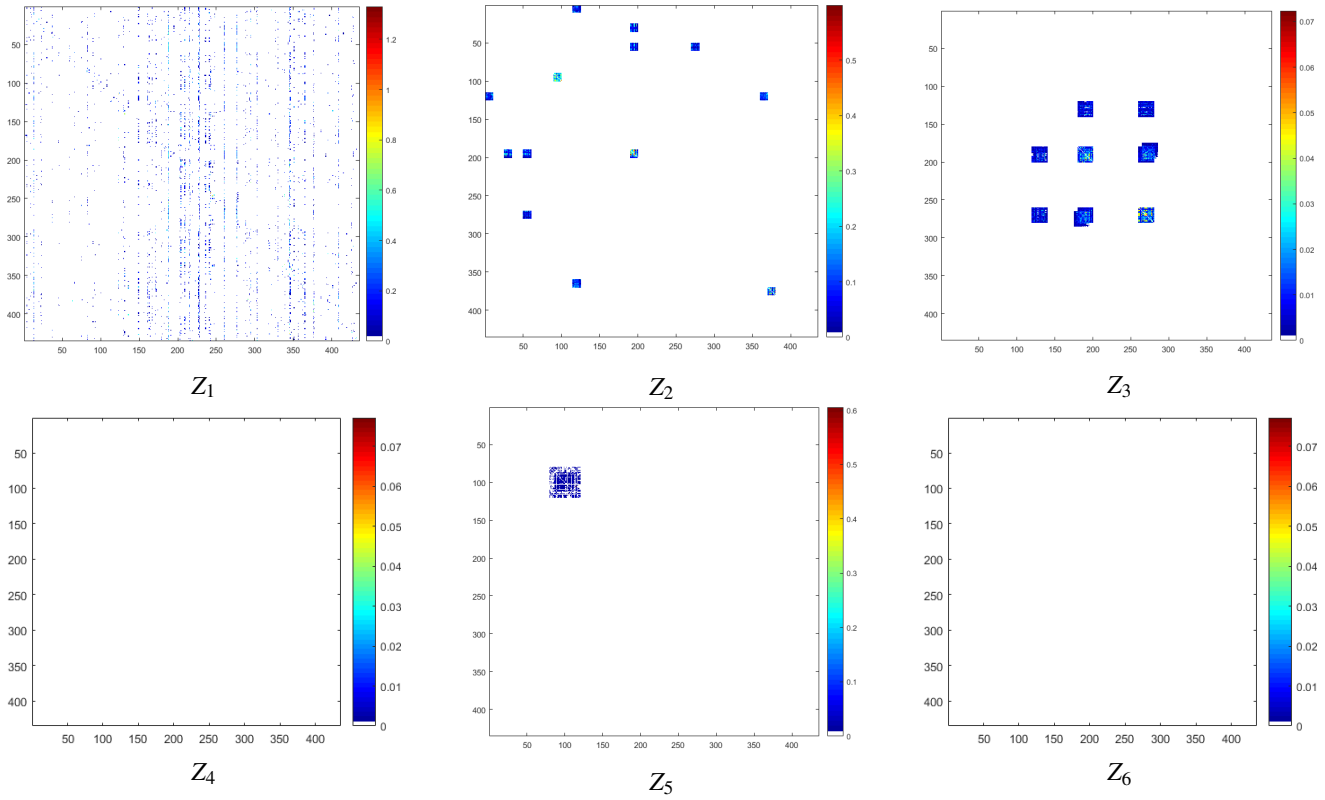


Figure 5: Heatmap of the structured precision matrix $\Theta$ decomposed into $Z_1 + \cdots + Z_6$ in the House voting data.

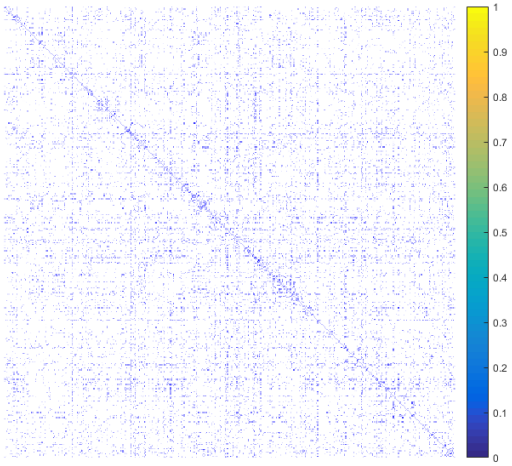

Figure 6: Heatmap of the inverse covariance matrix in the voting record of the U.S. House of Representatives, estimated by the graphical lasso method [17].

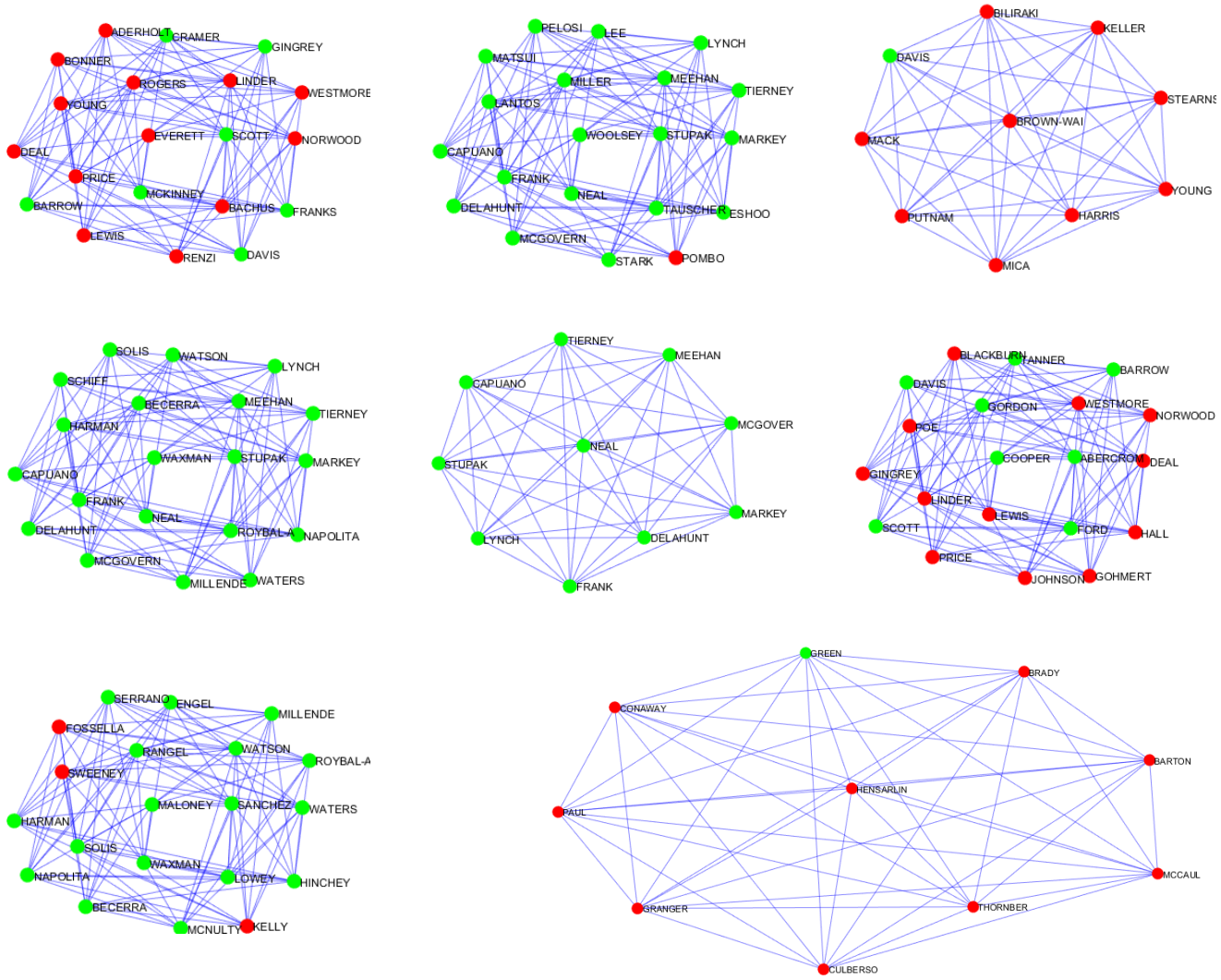


Figure 7: dense subgraphs identified by SGL for the House voting data with an inclusion cutoff value of 0.6. Subfigures corresponds to a densely connected area in Figure 5 for the symmetric structured matrix $Z_2$. The nodes represent House members, with red and green node colors corresponding to Republicans and Democrats, respectively. A blue line corresponds to an edge between two nodes.

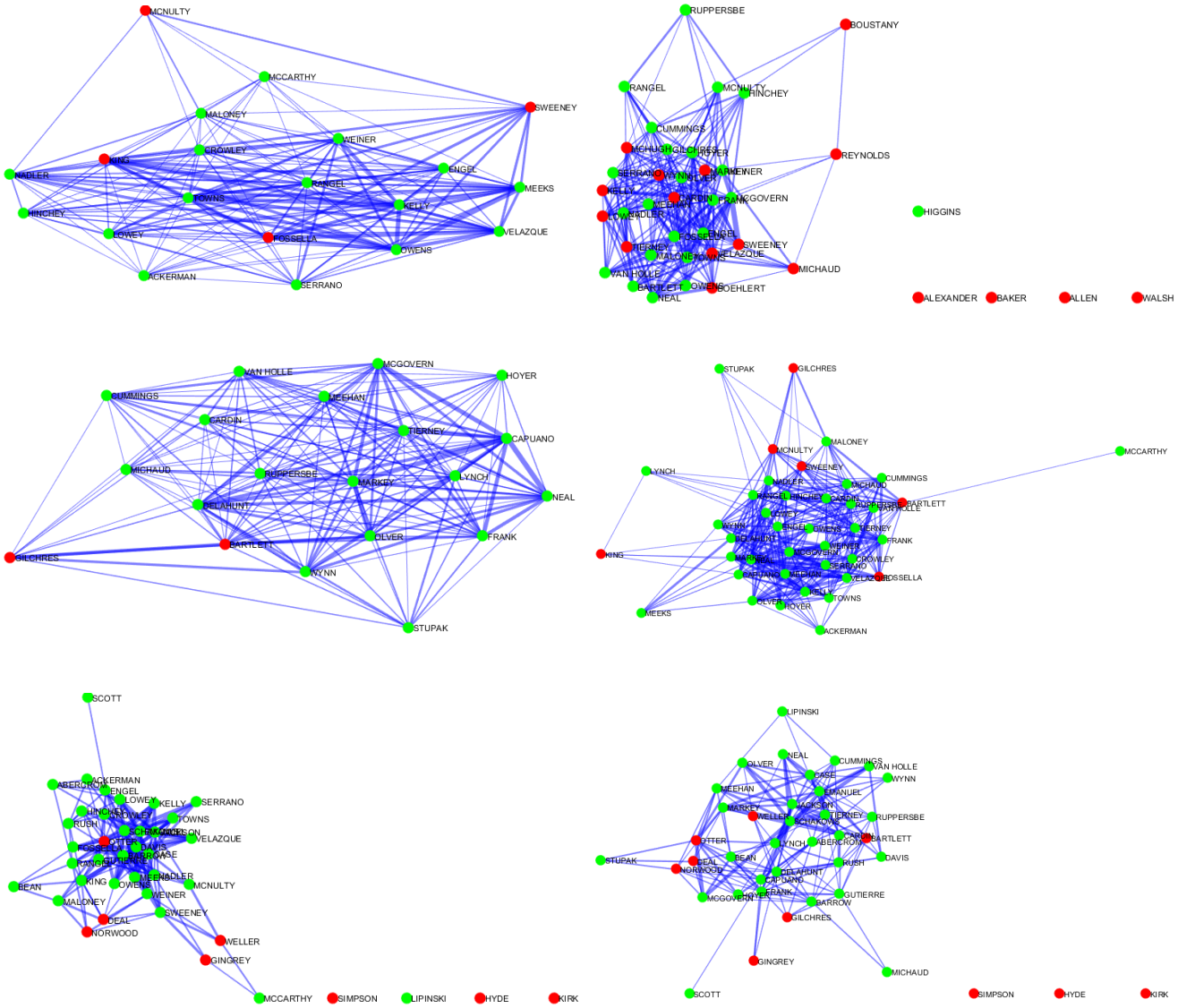


Figure 8: Locally correlated subgraphs identified by SGL for the Senate voting data with an inclusion cutoff value of 0.6. Subfigures corresponds to a densely connected area in Figure 5 for the symmetric structured matrix $Z_3$. The nodes represent House members, with red and green node colors corresponding to Republicans and Democrats, respectively. A blue line corresponds to an edge between two nodes.

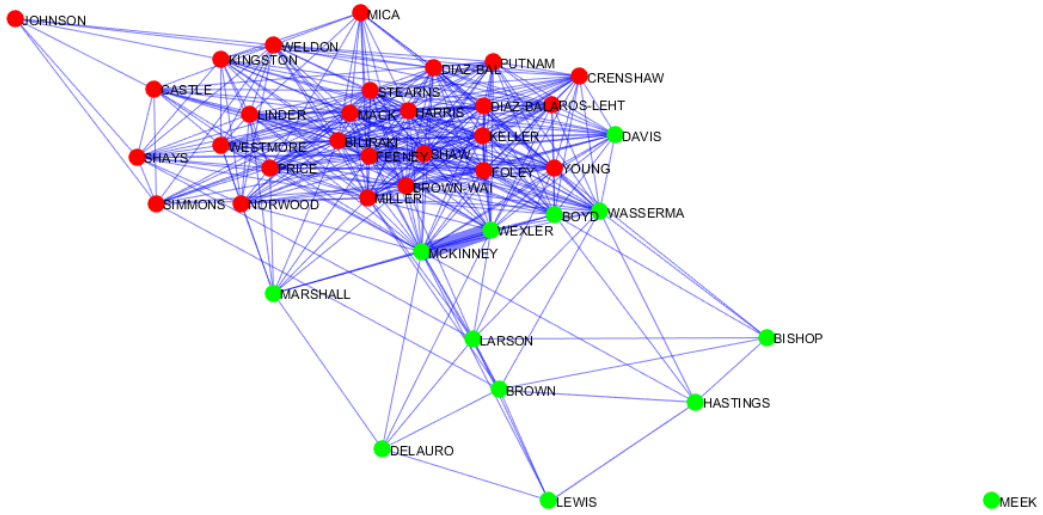


Figure 9: Dense subgraph identified by SGL for the House voting data with an inclusion cutoff value of 0.6. Subfigures corresponds to a densely connected area in Figure 5 for the symmetric structured matrix $Z_5$. The nodes represent House members, with red and blue node colors corresponding to Republicans and Democrats, respectively. A blue line corresponds to an edge between two nodes.

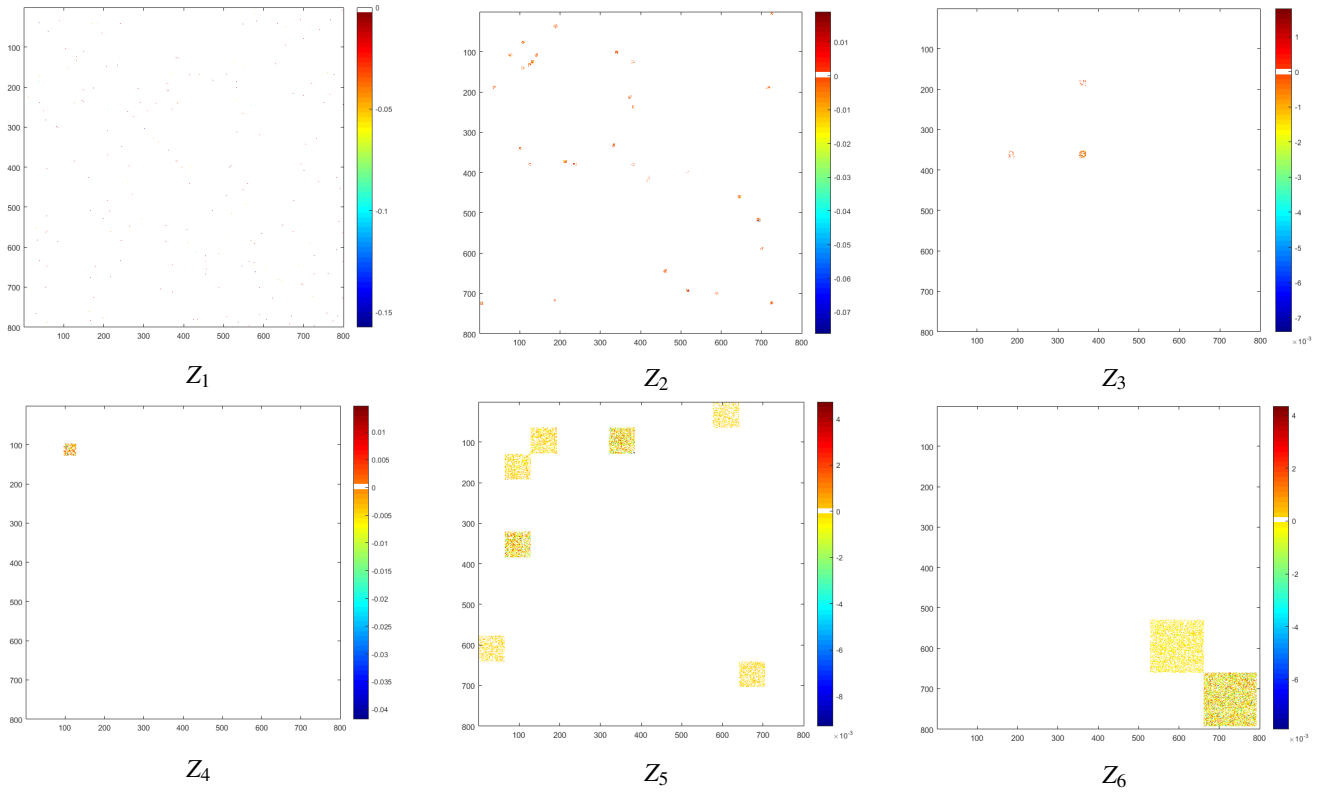


Figure 10: Heat map of the structured precision matrix $\Theta$ decomposed into $Z_1 + \cdots + Z_6$ in the breast cancer data set.

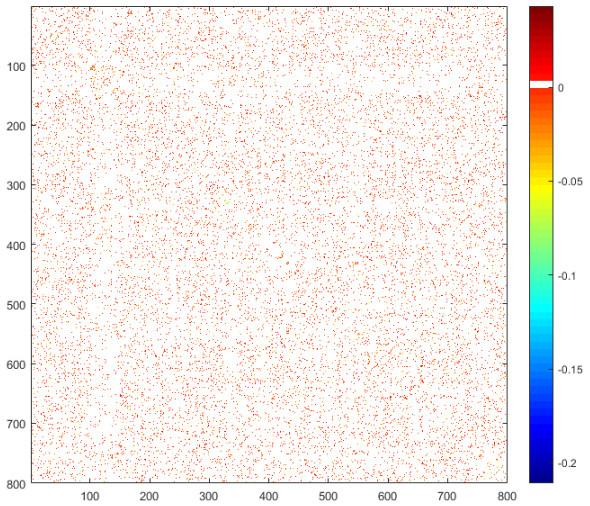

Figure 11: Heatmap of the inverse covariance matrix in the breast cancer data sets, estimated from graphical lasso [17].

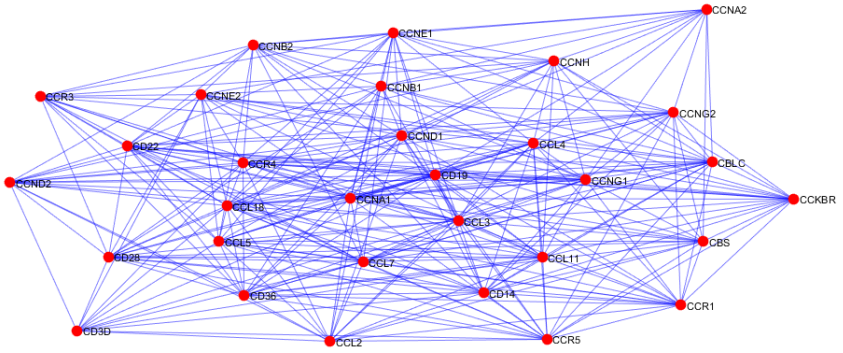


Figure 12: Network layout of grouped genes identified by SGL for the breast cancer data set. Subfigure corresponds to a densely connected area in Figure 10 for the structured matrix $Z_4$.

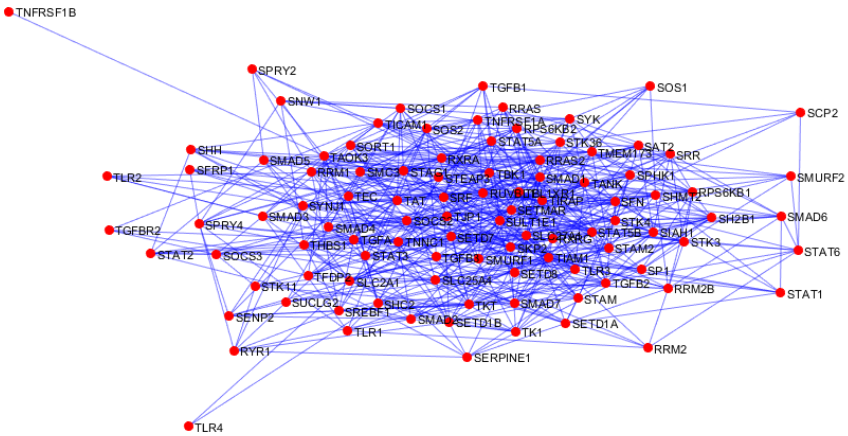


Figure 13: Network layout of grouped genes identified by SGL for the breast cancer data set. Subfigure corresponds to a densely connected area in Figure 10 for the structured matrix $Z_6$.

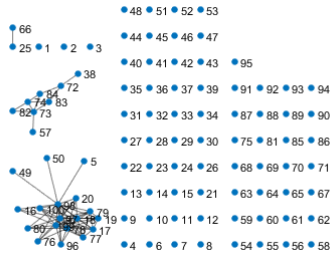

(a) Graphical lasso estimate [17]

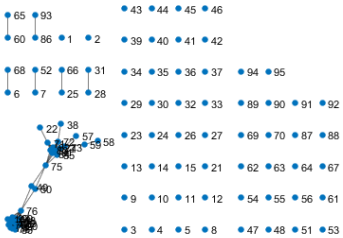

(b) Structured graphical lasso

(c) ground truth

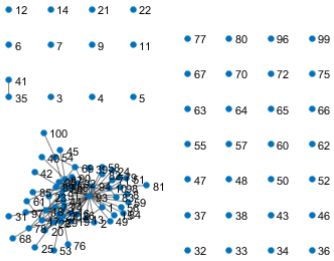

(d) Graphical lasso estimate [17]

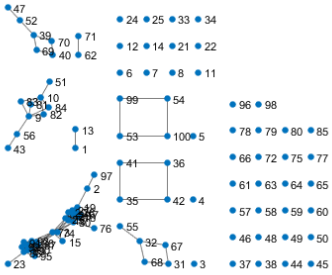

(e) Structured graphical lasso

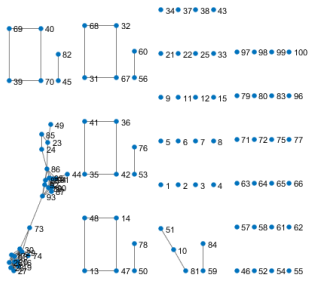

(f) ground truth

Figure 14: Simulation for the Gaussian graphical model. Row I: Results for $p = 100$ and $m = 200$. Row II: Results for $p = 100$ and $n = 50$.

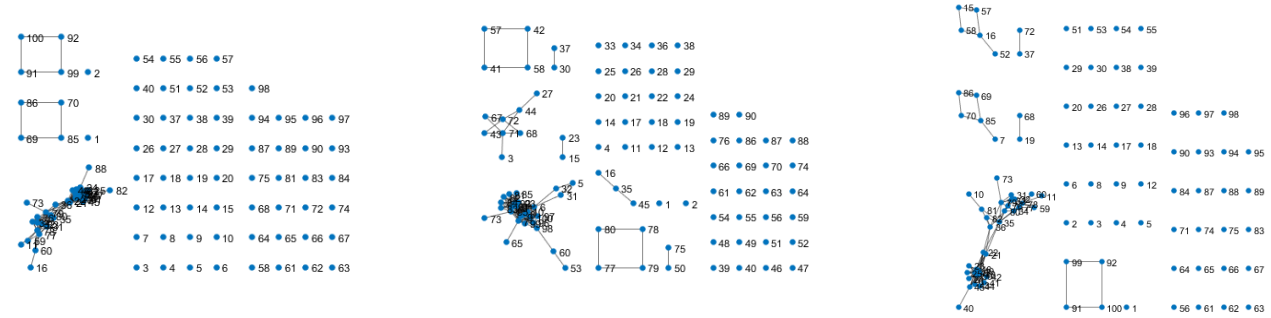

(a) Graphical lasso estimate [17]

(b) Structured graphical lasso

(c) ground truth

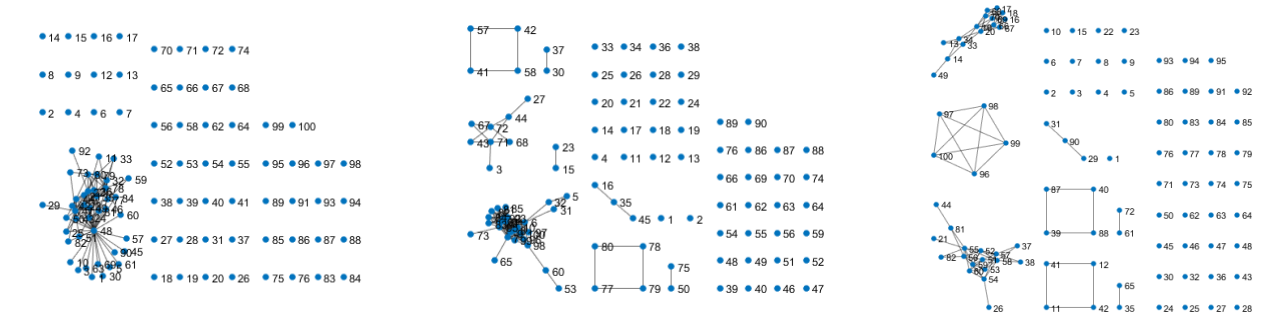

(d) Graphical lasso estimate [17]

(e) Structured graphical lasso

(f) ground truth

Figure 15: Simulation for the Covariance graph model. Row I: Results for $p = 100$ and $m = 200$. Row II: Results for $p = 100$ and $m = 50$.

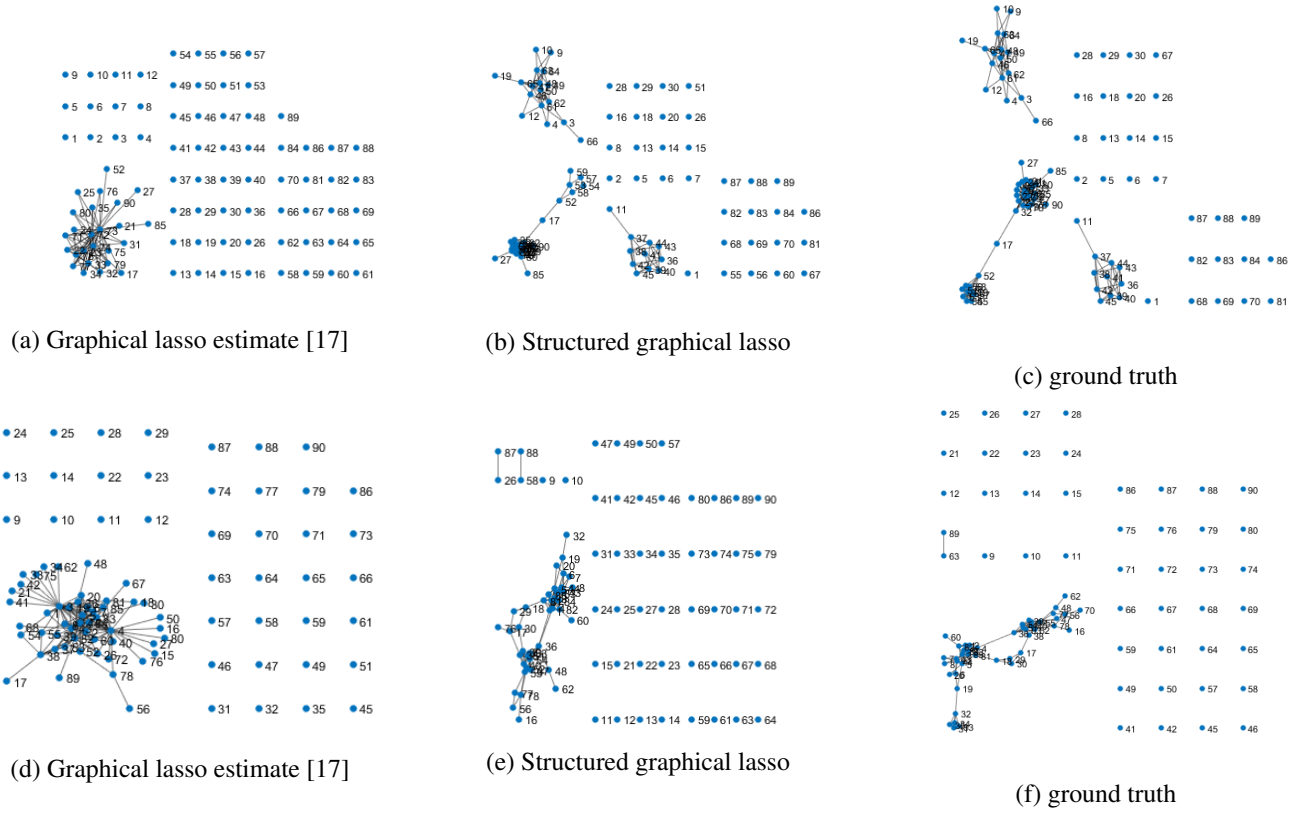

(a) Graphical lasso estimate [17]

(b) Structured graphical lasso

(c) ground truth

(d) Graphical lasso estimate [17]

(e) Structured graphical lasso

(f) ground truth

Figure 16: Simulation for the Gaussian graphical model with 10 latent variables. Row I: Results for $p = 100$ and $m = 200$. Row II: Results for $p = 100$ and $m = 50$.

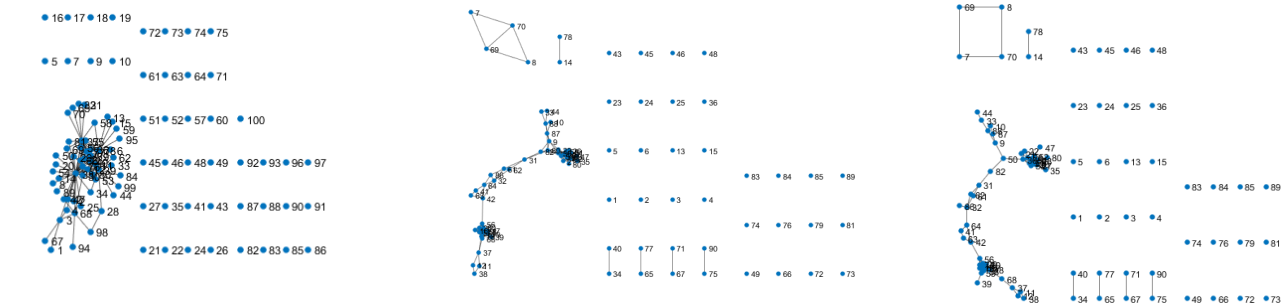

(a) Graphical lasso estimate [17]

(b) Structured graphical lasso

(c) ground truth

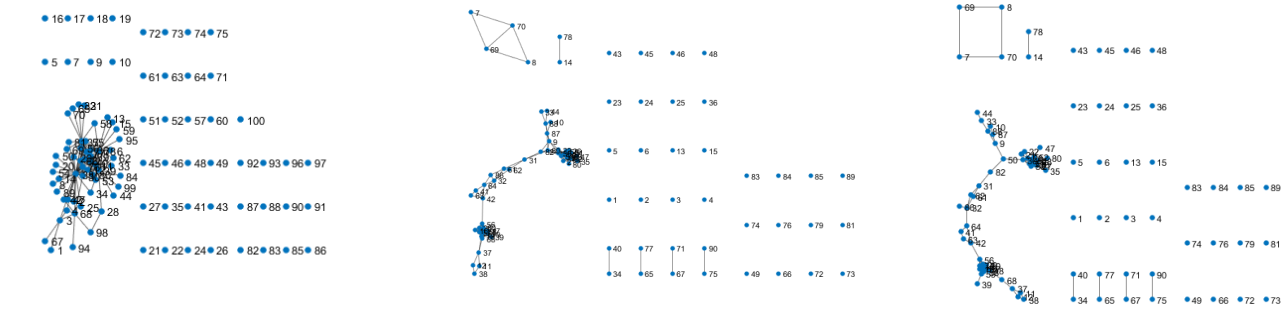

(d) Graphical lasso estimate [17]

(e) Structured graphical lasso

(f) ground truth

Figure 17: Simulation for the binary Ising Markov random field. Row I: Results for $p = 100$ and $m = 200$. Row II: Results for $p = 100$ and $m = 50$.